


12-2022

Synthesis and Biological Testing of Small-Molecule Mitochondrial Complex I Inhibitors

Willough Sloan
William & Mary

Follow this and additional works at: <https://scholarworks.wm.edu/honorstheses>

 Part of the [Biochemistry Commons](#), [Cancer Biology Commons](#), [Heterocyclic Compounds Commons](#), and the [Organic Chemicals Commons](#)

Recommended Citation

Sloan, Willough, "Synthesis and Biological Testing of Small-Molecule Mitochondrial Complex I Inhibitors" (2022). *Undergraduate Honors Theses*. William & Mary. Paper 1900.
<https://scholarworks.wm.edu/honorstheses/1900>

This Honors Thesis -- Open Access is brought to you for free and open access by the Theses, Dissertations, & Master Projects at W&M ScholarWorks. It has been accepted for inclusion in Undergraduate Honors Theses by an authorized administrator of W&M ScholarWorks. For more information, please contact scholarworks@wm.edu.

Synthesis and Biological Testing of Small-Molecule Mitochondrial Complex I Inhibitors



WILLIAM & MARY

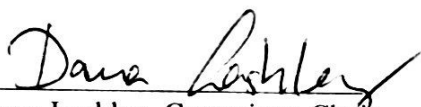
CHARTERED 1593

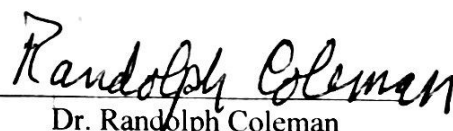
A thesis submitted in partial fulfillment of the requirement
for the degree of Bachelor of Science in Chemistry
from The College of William & Mary


by


Willough Sloan

Accepted for Honors


Dr. Dana Lashley, Committee Chair
Senior Lecturer of Chemistry
William & Mary


Dr. Randolph Coleman
Professor of Chemistry
William & Mary


Dr. Robert Pike
Professor and Department Chair of Chemistry
William & Mary


Dr. Oliver Kerscher
Associate Professor of Biology
William & Mary

Williamsburg, VA, USA
December 13th, 2022

TABLE OF CONTENTS

ACKNOWLEDGEMENTS.....	iii
ABBREVIATIONS	v
LIST OF FIGURES	vii
LIST OF SCHEMES	ix
LIST OF TABLES.....	x
ABSTRACT	1
1 INTRODUCTION TO MEDICINAL CHEMISTRY	2
1.1 MITOCHONDRIAL COMPLEX I INHIBITION IN DRUG DESIGN.....	2
1.2 SUBSTRATE-BASED INHIBITOR DESIGN.....	3
2 STUDIES INTO THE REGIOCHEMISTRY OF CHIMAPHILIN SYNTHESIS	5
2.1 INTRODUCTION TO NATURAL PRODUCTS	5
2.2 BIOLOGICAL SIGNIFICANCE AND SYNTHESIS OF CHIMAPHILIN	8
2.3 REGIOCHEMISTRY DETERMINATION USING X-RAY CRYSTALLOGRAPHY	11
3 QUINAZOLINE-BASED SMALL MOLECULE INHIBITOR EVP4593.....	16
3.1 MOTIVATION	16
3.2 SYNTHESIS OF EVP4593 DERIVATIVES	19
3.3 FUTURE EVP4593 DERIVATIVE SYNTHESSES	22
4 BIOLOGICAL TESTING OF EVP4593 AND DERIVATIVES.....	23
4.1 IN VIVO TESTING	23
4.2 IN VITRO TESTING.....	31
4.3 SIGNIFICANCE AND FUTURE PROSPECTS	34
5 SUPPLEMENTAL INFORMATION	34
5.1 Instrumentation and General Synthetic Procedures	34
5.2 Procedure for Synthesis of 3.9 (H-EVP1).....	35
5.3 Procedure for Synthesis of 3.10 (Br-EVP1).....	36
5.4 Procedure for Synthesis of 3.15 (F-EVP(A)1)	36
5.5 Procedure for Synthesis of 3.11 (Cl-EVP1).....	37
5.6 Procedure for Synthesis of 3.12 (I-EVP1).....	37
5.7 CRYSTALLOGRAPHIC INFORMATION	38
5.8 SPECTRAL INFORMATION	42
5.9 BIOLOGICAL METHODS	52
REFERENCES	54

ACKNOWLEDGEMENTS

When I consider the vast number of individuals who have been a blessing in my life – personally as well as academically – I realize I’m going to have to take up two pages here. I will start by thanking my major and research advisor, Dr. Dana Lashley. The start of the COVID-19 pandemic threw all of us into online learning through the winding and mysterious trenches of Blackboard, and it was here that I first learned anything from Dr. Lashley. I knew almost instantly that I wanted her to be my major advisor. After almost two years in her lab, I have found her to be a patient mentor, an excellent instructor and researcher, and an inspiration for the type of chemist I aspire to be.

From my time in Dr. Lashley’s laboratory, I learned that scientific research is highly collaborative. This research would have far less to say, and be less exciting, were it not for the substantial contributions of other researchers. For this reason, I would like to express my thanks to Dr. Hamid Nasiri for being the inspiration behind the EVP4593 SAR study, to Dr. Thorsten Friedrich and Jan Kaegi from the University of Hohenheim for the telling *in vitro* results, to Dr. Oliver Kerscher, Lexie Hiestand, and Stella Shen from William & Mary’s own SUMO Lab for the *in vivo* results (we had such a great time!), and Dr. Robert Pike for spending who knows how many hours looking at subpar crystals and working on the crystallography results (I think we had fun with it though). Although I could list almost the entire W&M chemistry department for their support and just for being wonderful people to be around, I want to especially thank Jeff Molloy, who has taught me more about a GC-MS than many people would care to know (but which is a true delight for a chemistry student). I also thank Dr. Randolph Coleman and Dr. Patricia Habersham for inspiring me beyond my understanding of myself as a scientist to realizing more and more my greater identity as a child of God. And, as a die-hard organic chemistry student, I

must thank the man who taught me my functional groups: Dr. Christopher Abelt, whose class I very much enjoyed and whose patience I very much required throughout the many random questions I threw at him throughout my time as an undergrad. I also thank the numerous friends at school and at home, at my church and within Agape Christian Fellowship, for their love and support throughout the years here at school. Thank you all, deeply.

I realized once I left them to go to college what a wonderful and strong family I have – my parents, Drs. Margaret and David Sloan, and my three siblings Lochinvar, Dulcinea, and Daniel. I thank the glorious God for them, their genuine love, and their blunt honesty (what can I say – the Sloans are a rough crowd). I am sorry to inform my siblings that, sadly, H-EVP1 was not first synthesized by me, so I don't get to name it (although I appreciated the suggestion to call one of my molecules "Lightning McQueen" in honor of our siblinghood, in reference to the strange love of the Pixar movie *Cars* that we all share). And if you want to know someone who greatly upheld me in the grueling process of writing a thesis, I will tell you about my precious sister in Christ and roomie, Athena Liao, who supported me with food and Bible verses. In fact, many people brought me food, so perhaps I ought to write theses more often.

And lastly, I thank my God. It is beyond my understanding to fully comprehend the love that brought Jesus down to earth and allowed Him to die in place of sinful humanity, opening a door of life to all who will accept the now-resurrected Jesus as their Savior. I did not want to be a Christian, but God caught my heart anyway. Now, I just love Him, and I *want* to follow Him. This is the patient and relentlessly loving God I dedicate my thesis (and life) to: the Lord Jesus Christ, "who loved me and gave Himself for me" (Galatians 2:20).

ABBREVIATIONS

ATP	Adenosine triphosphate
br	Broad
d	Doublet
DCM	Dichloromethane
dd	Doublet of doublets
DMSO	Dimethyl sulfoxide
EA	Ethyl Acetate
ETC	Electron Transport Chain
FDA	US Food and Drug Administration
eq	Equivalents
g	Grams
GC	Gas Chromatography
G/E	Glycerol/Ethanol
h	Hours
Hex	n-Hexane
m	Multiplet
M	Molarity
MCI	Mitochondrial Complex I
m/z	Mass to charge ratio
min	Minutes
ml	Milliliter
mmol	Millimole

mol	Mole
MS	Mass Spectrometry
NADH	Nicotinamide adenine dinucleotide
NMR	Nuclear Magnetic Resonance
q	Quartet
RT	Room temperature
s	Singlet
t	Triplet
THF	Tetrahydrofuran
TLC	Thin-Layer Chromatography
YEP	Yeast extract peptone
YPD	Yeast extract peptone dextrose
XRD	X-ray diffraction
96W	96 well

LIST OF FIGURES

Figure 1.1. The Electron Transport Chain in mitochondria ⁶	2
Figure 1.2. An example of a typical IC ₅₀ curve ⁷	4
Figure 1.3. Natural Product Derivatives synthesized for Substrate Based Inhibitor Design ⁸	4
Figure 2.1. Number of worldwide approved small molecule drugs per year that are natural products (N), botanical drugs (NB), natural product derivatives (ND), or synthetic drugs with a natural product pharmacophore (S*) ¹⁰ . “201909” denotes that the count went until September 2019.....	6
Figure 2.2. Chemical structures for aspirin, sulforaphane, and paclitaxel.....	7
Figure 2.3. Some common quinones.....	8
Figure 2.4. Examples of quinone-containing structures found in nature.....	9
Figure 2.5. Chimaphilin and its regioisomer.....	10
Figure 2.6. Chimaphilin and structural proxy 2.11	13
Figure 2.7. The chimaphilin dimer shown from different angles.....	13
Figure 2.8. The co-crystallized isomeric structure, with the C6-methyl isomer labeled as “A” atoms and the C7-methyl isomer labeled as “B” atoms. “B” atoms have been highlighted to help show structure of the C7-methyl isomer and are somewhat disorderly in the structure due to low diffraction density.....	15
Figure 3.1. Chemical structure of EVP4593.....	16
Figure 3.2. Examples of anticancer drugs with quinazoline moiety. Substructure identical to the quinazoline core of EVP4593 is shown in blue.....	18
Figure 3.3. Structures of Selinexor, Apalutamide, and Alpelisib.....	19
Figure 3.4. The numbered quinazoline ring.....	20
Figure 3.5. Basic chemical skeleton of future planned derivatives. Locations of specific structural changes highlighted in blue.....	23
Figure 4.1. Time of sampling v. WT <i>S. cerevisiae</i> growth at given EVP4593 concentrations. After 12 hours a significant difference (p<0.01) was seen for all tested EVP4593 concentrations. “NT” indicates no treatment (control).	24
Figure 4.2. Electron microscopy images of <i>pdr5Δ</i> cells, both untreated (left) and EVP4593-treated (right). Mitochondria are tagged with a red fluorescent protein (su9-RFP), septin rings are tagged with yellow fluorescent protein (YFP), and vacuoles are visualized using FM4-64 staining.....	25
Figure 4.3. Box and whisker plots showing the diameter of <i>pdr5Δ</i> cells (top) and septin rings (bottom). Treatment lasted for 6 hours. A single-factor ANOVA test was used (>p=0.001*).	26
Figure 4.1. A serial dilution spotting assay showing the strains most sensitive to EVP4593. Strain <i>ara2Δ</i> is a positive control, while <i>sod2Δ</i> is a negative control. Each consecutive spot represents a ten-fold dilution.	27
Figure 4.2. EVP4593 tested against Br-EVP1. “/” indicates the standard YEP G/E media, “E” indicates treatment with EVP4593 (15 μM), and “*” indicates treatment with Br-EVP1 (15 μM).	28
Figure 4.3. H-EVP1, I-EVP1, and F-EVP(A)1 tested against each other. “/” indicates the standard YEP G/E media, “I” indicates treatment with I-EVP1 (15 μM), “H” indicates treatment with H-EVP1 (15 μM), and “F” indicates treatment with F-EVP1 (15 μM).	29
Figure 4.4. Frequency of ~20 sensitive mutant phenotypic associations.....	30
Figure 4.5. Results from treating various in-membrane oxidases with H-EVP1. (A-B) Image of a cell with complexes I, NDH-II, <i>bd-I</i> , and <i>bd-II</i> boxed; IC ₅₀ plot for H-EVP1 against <i>E. coli</i> NADH oxidase. (C-D) Image of cell with complexes I, <i>bd-I</i> , and <i>bd-II</i> boxed; IC ₅₀ plot for H-EVP1 against <i>E. coli</i>	

dNADH oxidase. (E-F) Image of cell with succinate dehydrogenase (SDH) and complexes <i>bd</i> -I and <i>bd</i> -II boxed; IC ₅₀ plot for H-EVP1 against <i>E. coli</i> succinate oxidase.....	32
Figure 4.6. Results from treating isolated <i>bd</i> -I and <i>bd</i> -II oxidases with H-EVP1.	33
Figure 4.7. Results from treating isolated <i>bd</i> -I and <i>bd</i> -II oxidases with Br-EVP1.	33
Figure 5.1. ¹ H-NMR spectrum of H-EVP1.	43
Figure 5.2. Zoom of ¹ H-NMR aromatic region of H-EVP1.....	43
Figure 5.3. ¹³ C-NMR spectrum of H-EVP1.....	44
Figure 5.4. ¹ H-NMR spectrum of Br-EVP1.....	45
Figure 5.5. Zoom of ¹ H-NMR aromatic region of Br-EVP1.....	45
Figure 5.6. ¹³ C-NMR spectrum of Br-EVP1.....	46
Figure 5.7. ¹ H-NMR spectrum of F-EVP(A)1.	47
Figure 5.8. Zoom of ¹ H-NMR aromatic region of F-EVP(A)1.....	47
Figure 5.9. ¹³ C-NMR spectrum of F-EVP(A)1.	48
Figure 5.10. ¹ H-NMR spectrum of Cl-EVP1.	49
Figure 5.11. Zoom of ¹ H-NMR aromatic region of Cl-EVP1.....	49
Figure 5.12. ¹³ C-NMR spectrum of Cl-EVP1.	50
Figure 5.13. ¹ H-NMR spectrum of I-EVP1.....	51
Figure 5.14. Zoom of ¹ H-NMR aromatic region of I-EVP1.	51
Figure 5.15. ¹³ C-NMR spectrum of I-EVP1.	52

LIST OF SCHEMES

Scheme 2.1. The solvent-mediated reaction producing chimaphilin (2.10) and 1.1 shown here side by side with the plants that are their natural sources ^{23,24}	10
Scheme 2.2. Proposed [2+2] cycloaddition reaction of chimaphilin.	14
Scheme 2.3. Synthesis of phenyl chimaphilin.	14
Scheme 3.1. Generalized reaction sequence for Series 1 EVP4593 derivatives.	20
Scheme 3.2. EVP4593 derivative reaction mechanism. The “R” group represents either the H, Br, F, Cl, or I substituents.	22

LIST OF TABLES

Table 2.1. Attempted crystallization methods. The two entries highlighted in blue produced crystals and are discussed in more detail below.	12
Table 3.1. Physical attributes of synthesized EVP4593 derivatives.	21
Table 3.2. Series 1-3 of EVP4593 SAR analysis. Compounds that have been fully synthesized are highlighted in blue.	23
Table 4.1. Oxidase IC ₅₀ values tested against H-EVP1 and Br-EVP1.	33
Table 5.1. Crystal data and structure refinement for both the chimaphilin dimer and the phenyl chimaphilin.	38
Table 5.2. Bond lengths [Å] and angles [°] for the chimaphilin dimer structure.	39
Table 5.3. Bond lengths [Å] and angles [°] for the phenyl chimaphilin structure.	40

ABSTRACT

This thesis delineates two main projects: the first outlines the structure elucidation efforts toward a Diels-Alder adduct of a novel reaction for the synthesis of chimaphilin, a naphthoquinone-based natural product with apoptotic or antiproliferative activity in certain cancer cells^{1,2}. The structure elucidation extends to derivatives of chimaphilin synthesized by the same cyclization reaction. While Diels-Alder reactions are usually regioselective, ¹H-NMR and ¹³C-NMR of the adducts was inconclusive and indicated the possibility of regioisomer presence, with one regioisomer being chimaphilin (or derivatives). A multitude of crystallization methods were carried out in order to be able to analyze the products via X-ray crystallography. An unusual chimaphilin [2+2] cycloaddition dimer was discovered, indicating the correct positioning of the methyl group at C6 of the naphthoquinone scaffold. A phenyl derivative of chimaphilin was also crystallized to reveal a mixture of regioisomers with substituents positioned at C6 or C7 respectively.

The second project marks the auspicious beginnings of a Structure-Activity Relationship (SAR) study based on hit compound EVP4593, a known mitochondrial complex I (MCI) inhibitor³. The intention of this SAR study is the design of an improved MCI inhibitor for use as a potential anticancer agent. A series of derivatives of EVP4593 were synthesized, purified, and analyzed spectroscopically. Biological testing was conducted both *in vitro* on in-membrane NADH, succinate, and dNADH oxidases and on isolated *bd*-I and *bd*-II oxidases from *Escherichia coli* (*E. coli*) and *in vivo* against a genetic knockout library of >5100 *Saccharomyces cerevisiae* (*S. cerevisiae*) strains, revealing that the compound titled “H-EVP1” was the most potent inhibitor out of the tested EVP4593 derivatives and was possibly selective for MCI when compared to other oxidases.

1 INTRODUCTION TO MEDICINAL CHEMISTRY

1.1 MITOCHONDRIAL COMPLEX I INHIBITION IN DRUG DESIGN

The field of organic chemistry has much to offer medicine, whether it be by providing a better understanding of the many organic compounds that play a role in biological systems or through the identification of novel or improved therapies. Indeed, Wess et al.⁴ stated that “excellent organic chemists are vital to put the concept of chemical biology into practice”, identifying organic synthesis as one of two directions important for the future of drug design.

NADH:ubiquinone oxidoreductase, also known as mitochondrial complex I (MCI), is the largest and least understood complex in the series of protein complexes comprising the Electron Transport Chain (ETC) in eukaryotic mitochondria⁵. MCI shuffles electrons from coenzyme NADH to ubiquinone (also known as coenzyme Q10), building up the proton electrochemical gradient necessary for ATP synthesis⁵. ATP is the energy currency of cells necessary for all forms of cellular work required to sustain life. Oxidative phosphorylation via the ETC produces the vast majority of ATP in eukaryotic cells.

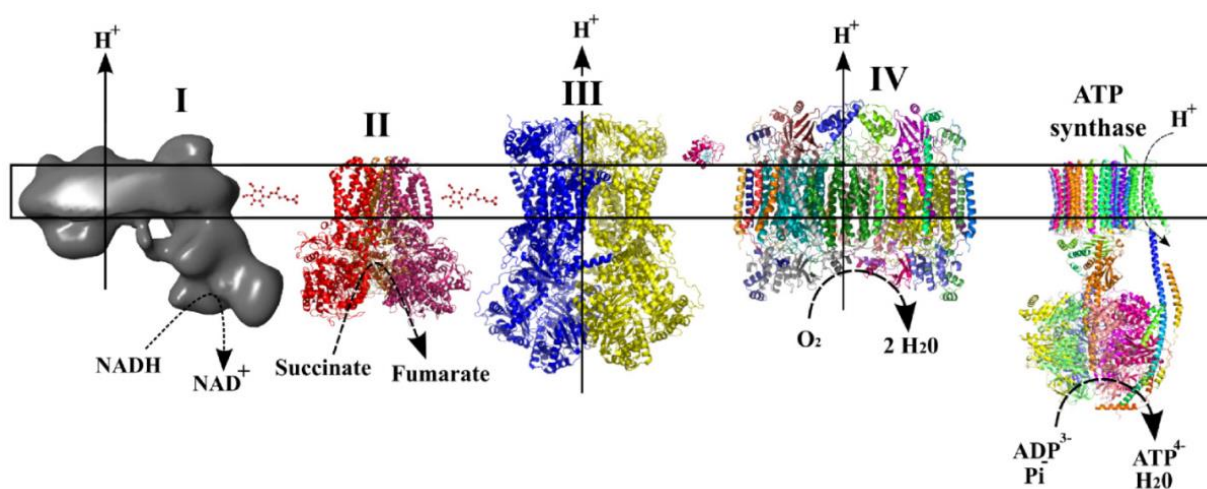


Figure 1.1. The Electron Transport Chain in mitochondria⁶.

Small-molecule inhibitors bind to the target enzyme, blocking the normal substrate – in the case of MCI, Q10 – from binding, either by physically occupying the enzyme’s active site or by inducing a conformational change that prevents substrate active site binding. Preventing the substrate from binding essentially shuts down enzyme function. Effective MCI inhibition therefore obstructs the entire ETC reaction cascade, thus preventing ATP production via oxidative phosphorylation. For this reason, MCI inhibitors are of interest as potential anticancer drugs, as tumorigenic cells require heightened amounts of ATP to feed uncontrolled division. Removing the major source of ATP, then, effectively “starves” a cancer cell.

1.2 SUBSTRATE-BASED INHIBITOR DESIGN

Inhibitor design begins with a biological Catch-22: in order to inhibit a target enzyme, effective inhibitors must first be capable of interacting with the target enzyme. An inhibitor that cannot bind to the enzyme will not be able to inhibit it, but an inhibitor that behaves too much like the original substrate may not have the strong inhibitory effects desired in a potential drug candidate. Substrate-based inhibitor design focuses on creating structural derivatizations of an enzyme’s normal substrate in order to identify chemical substructures that resemble the substrate which enable binding to the enzyme while introducing new moieties that lead to enzymatic inhibition.

Inhibition is typically measured as an IC_{50} (half-maximal inhibitory concentration). The binding response to a molecule is often a sigmoidal curve as seen in Figure 1.2; the IC_{50} is the value in the middle of the curve. Thus, smaller IC_{50} values correspond to better inhibitors, indicating a lower effective concentration.

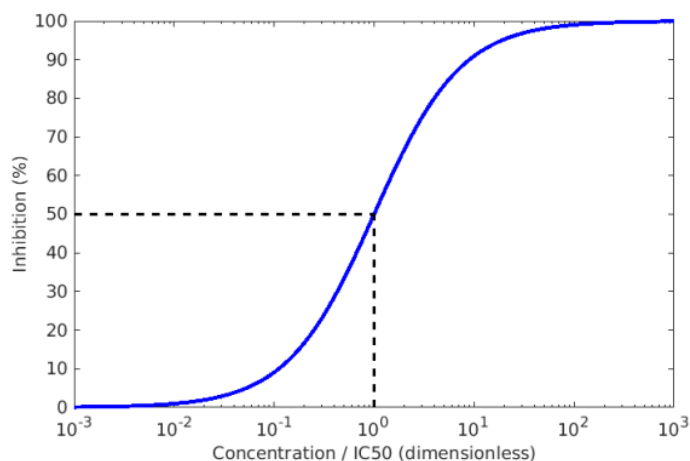


Figure 1.2. An example of a typical IC_{50} curve⁷.

A good example of substrate-based inhibitor design is found in a synthesis previously performed by our lab. A series of derivatives of a natural product from *Pyrola media* (**1.1**) were tested for their inhibitory activity versus MCI. The most promising inhibitors were compounds **1.2** and **1.3** (Figure 1.3). Structural elements from inhibitors **1.2** ($IC_{50}=8.9\mu M$) and **1.3** ($IC_{50}=238\mu M$) were then combined to produce **1.4**, a better inhibitor than either of its two precursors with an IC_{50} of $5.2\mu M$ ⁸.

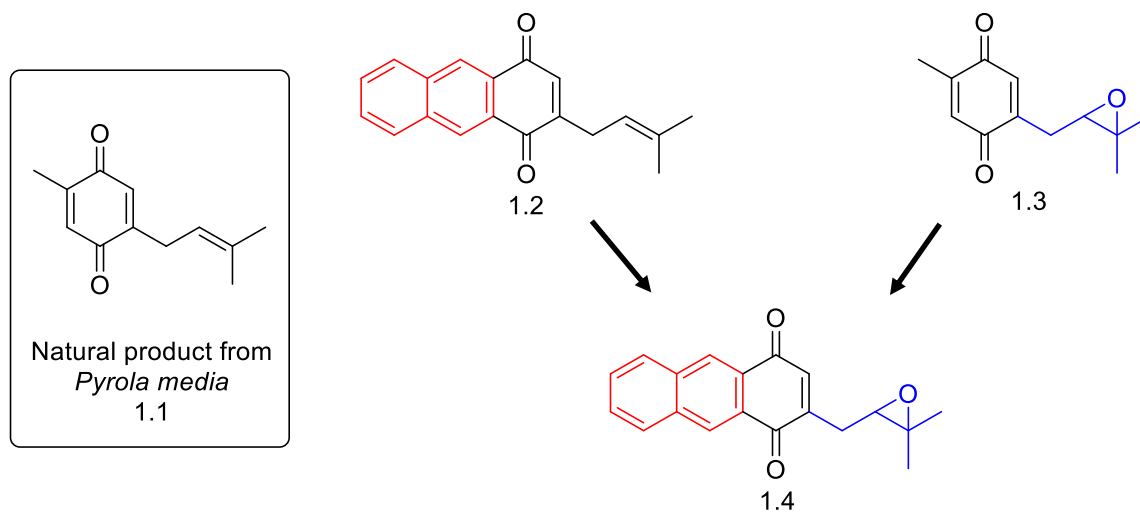


Figure 1.3. Natural Product Derivatives synthesized for Substrate Based Inhibitor Design⁸.

2 STUDIES INTO THE REGIOCHEMISTRY OF CHIMAPHILIN SYNTHESIS

2.1 INTRODUCTION TO NATURAL PRODUCTS

Natural products are organic molecules synthesized by living organisms, typically as secondary metabolites, described as “an excellent source of complex chemicals with a wide variety of biological activities”⁹. Natural products have unique structural features that vary greatly among different organisms. The connection to living organisms and the interesting structural diversity make natural products intriguing to medicinal chemists; indeed, there is good reason for this interest as many natural products have been shown to have beneficial physiological effects, including antibacterial, antifungal, anticancer, antiviral, and antiparasitic activities¹⁰.

Plant-based medicines have been used for millennia, with the first surviving written records of Mesopotamian medicine – written in cuneiform script on clay tablets – dating as far back as 2600BC¹¹. It was not until much later, in the early 19th century, that humans started isolating the active ingredients of plants to make much more potent drugs than the plants from which they were derived. Friedrich Sertürner, a German scientist who first isolated morphine from *Papaver somniferum*, overdosed on the substance¹², not realizing how much more potent it was in its pure isolated form. Unlike morphine, most natural products are not produced by the organism in large quantities as they serve secondary metabolic roles and are not essential for cell growth and reproduction. Investigating natural products is useful for medicinal chemists as it not only enables the identification of molecular structures responsible for particular medicinal outcomes but also allows for the discovery of efficient laboratory syntheses for larger-scale production of these molecules. Additionally, there is an open potential to increase natural product effectiveness through derivatization.

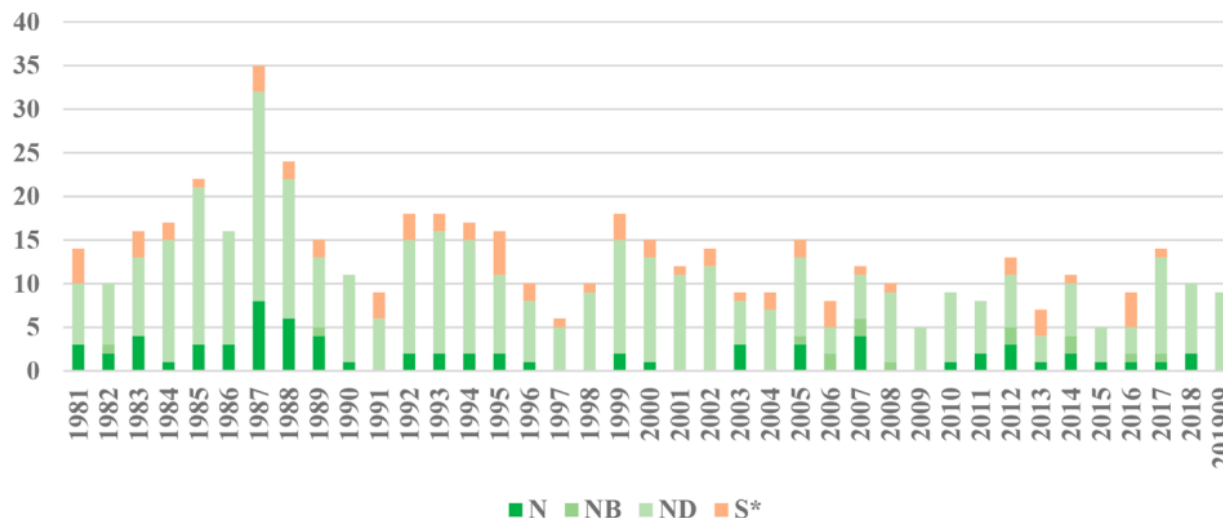


Figure 2.1. Number of worldwide approved small molecule drugs per year that are natural products (N), botanical drugs (NB), natural product derivatives (ND), or synthetic drugs with a natural product pharmacophore (S*)¹⁰. “201909” denotes that the count went until September 2019.

The potential seen in natural products is validated by the existence of the US National Cancer Institute’s (NCI) Natural Product Repository, which holds over 230,000 natural product extracts¹³. In January of 2019 NCI’s Program for Natural Product Discovery (NPNPD), under the Division of Cancer Research and Diagnosis (DCTD), launched its prefractionated (separated out prior to biological testing) library that now has over 326,000 extracts available, with the hope that this library will make natural products, identified as “[i]mportant sources of new drugs and drug leads”, more amenable to high-throughput screening¹⁴. Natural products are also attractive alternatives to purely synthetic medicines as therapeutics that potentially lessen side effects¹⁵.

A famous natural product-based medicine is found on pharmacy shelves everywhere – aspirin (acetylsalicylic acid, **2.1**), originating in the salicylates directly synthesized in Willow bark and known for its anti-inflammatory (via prostaglandin synthesis inhibition) and blood thinning properties¹⁶. Sulforaphane (**2.2**), a natural product isolated from broccoli (*Brassica oleracea*), is a potential therapeutic against Alzheimer’s, stroke, depression, multiple sclerosis,

and other health issues, with positive effects recorded in animal models¹⁷. Taxol – the natural product paclitaxel, **2.3** – is an anticancer drug isolated from the bark of the Pacific Yew (*Taxus brevifolia*) that affects normal microtubule functioning⁹, now with over 12 total syntheses¹⁸.

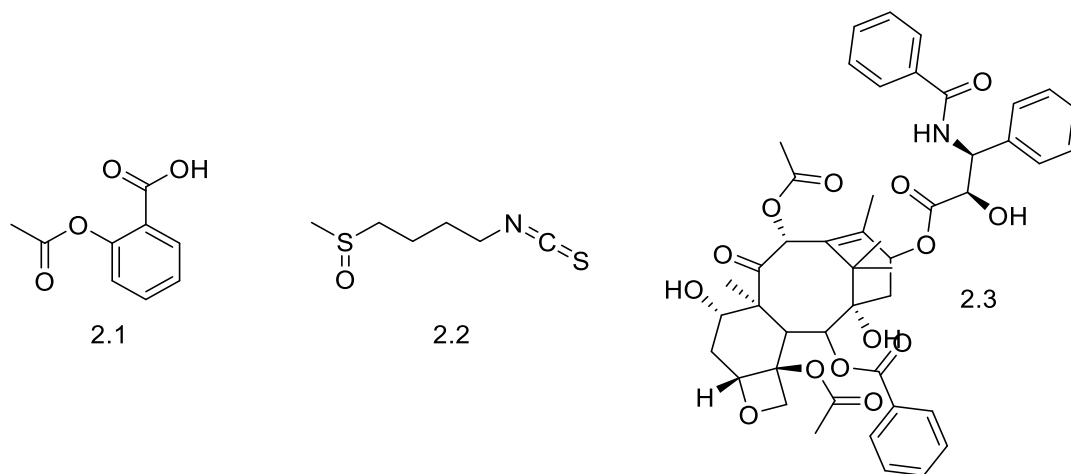


Figure 2.2. Chemical structures for aspirin, sulforaphane, and paclitaxel.

Taking advantage of the promising biological effects necessitates the discovery of reliable laboratory syntheses for these natural products to be of any practical use. Early stages in biological testing may only require milligram-scale amounts of a compound, but more extensive testing – and certainly viability as a marketable drug – requires such amounts (grams or even kilograms) as are typically not produced in nature (they are secondary metabolites, after all). Harvesting natural products directly from the organism also raises concern over the environmental impact and renewability of source materials. In the case of Taxol, although the prolific amount of Pacific Yew trees initially eased environmental worries, in the years 1991 and 1992 over 1.6 million pounds of bark was harvested annually⁹. Harvesting the bark does kill the tree, however, and in 2011 the International Union for Conservation of Nature and Natural Resources had classified another type of yew, *Taxus contorta*, as endangered, in part due to overharvesting¹⁹. When a renewable natural source was discovered – needles from the English

Yew (*Taxus baccata*) – it still required laboratory organic technique to convert the natural product into the final drug product⁹. Taxol is a case in point that natural products, though promising, generally require some synthetic laboratory input to be viable drug agents. Today, Taxol is a standard chemotherapy agent used in the treatment of breast, lung, ovarian, and other types of cancers⁹, and constitutes one of the most important anticancer drugs ever produced.

2.2 BIOLOGICAL SIGNIFICANCE AND SYNTHESIS OF CHIMAPHILIN

Quinones are a class of organic molecules that are ubiquitous in nature. A quinone features a conjugated diketone ring structure with electrophilic sites located at the carbonyl carbons as well as at the beta-positions. Quinone functions in nature are related to their redox activity; according to El-Najjar et al.²⁰, the chemical importance of quinones in biological systems stems from their potential for one or two electron reduction and to serve as electrophiles for nucleophilic attack. Some examples of this class are shown below: 1,4-Benzoquinone, 1,2-Benzoquinone, 1,4-Naphthoquinone, and 1,4-Anthraquinone.

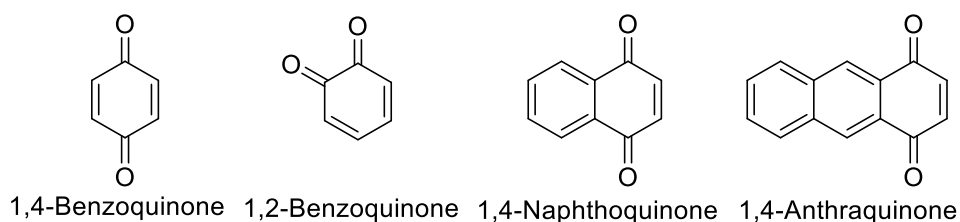


Figure 2.3. Some common quinones.

Quinones are very abundant in nature²⁰. Indeed, the natural substrate for MCI is a quinone called coenzyme Q10, or ubiquinone (**2.4**)⁵. Another example is Thymoquinone (**2.5**), a natural product from *Nigella sativa* seeds, which is noted to have antitumor, anti-inflammatory, and antimicrobial effects, as well as neuroprotective effects¹⁵. These natural product quinones can

range from the more simplistic – such as thymoquinone – to the relatively complex, such as doxorubicin (**2.6**), a well-known FDA-approved chemotherapy drug that is synthesized naturally by bacterium *Streptomyces peucetius*²¹. The Vitamin K compound family is linked not only to blood coagulation but also to connective tissue calcification and cardiovascular health²²; phyloquinone (**2.7**), also known as Vitamin K1, is naturally produced in many green plants and is in high demand as a dietary supplement, creating an impetus to synthesize and otherwise manufacture this compound²². Due to their important biological function, many quinones are also interesting medicinally.

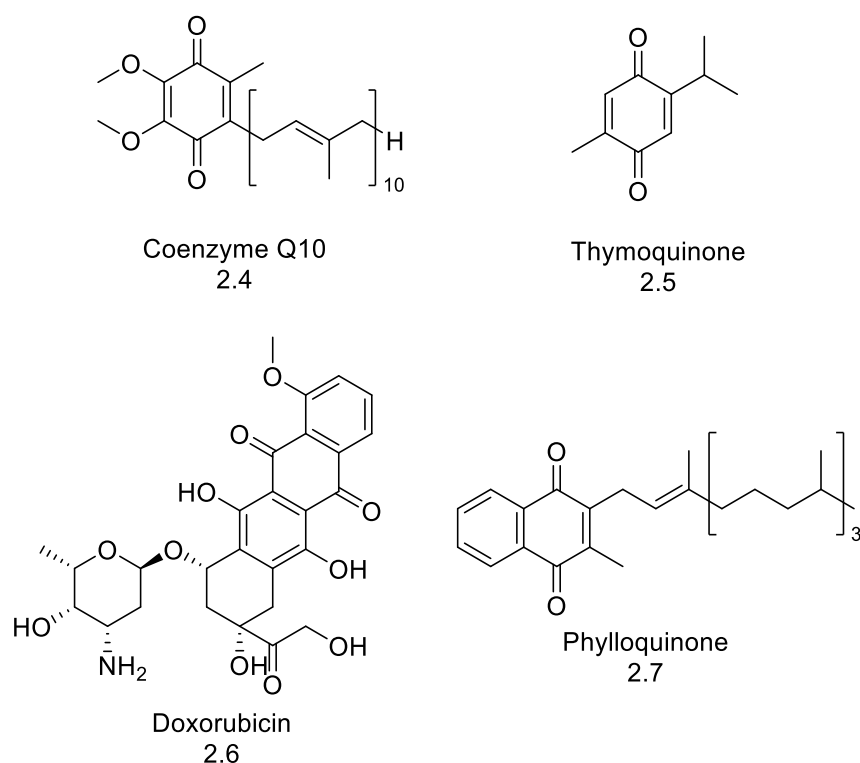
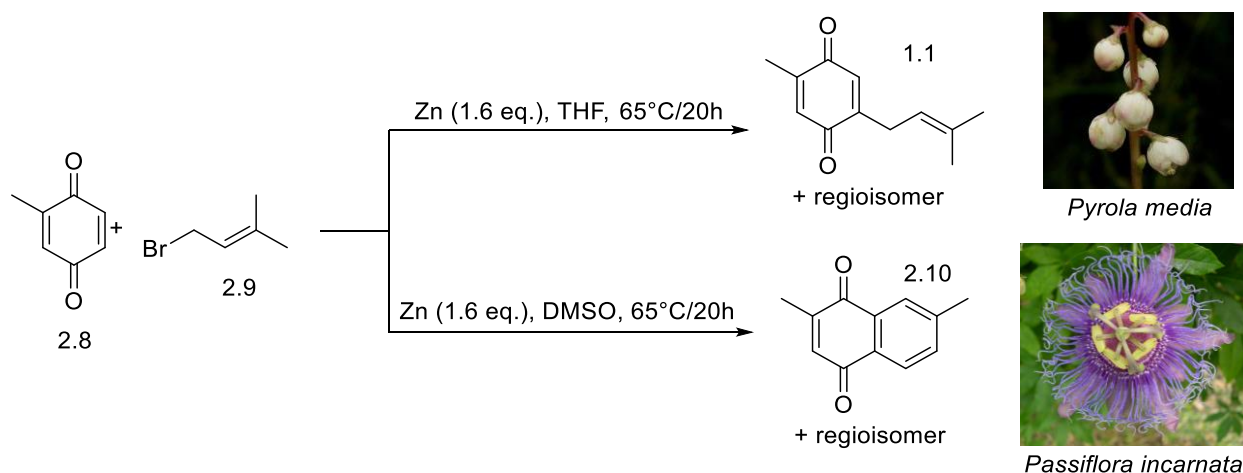


Figure 2.4. Examples of quinone-containing structures found in nature.

Because of their numerous appearances in biological contexts, natural product quinone substrates are excellent starting points for substrate-based inhibitor design for enzymes with quinone substrates. Towards this end, our lab had previously uncovered a solvent-dependent reaction

whereby a THF-mediated reaction produced 2-methyl-5-prenyl-1,4-benzoquinone (**1.1**), a natural product from the plant *Pyrola media*⁸. It was discovered that, by changing only the reaction solvent from THF to DMSO, a new product – 2,7-dimethylnaphthalene-1,4-dione (**2.10**) – was formed. **2.10**, also known as chimaphilin, is a natural product from the flower *Passiflora incarnata*¹. Chimaphilin has reported apoptotic activity against human breast cancer (MCF-7) cells and preventative activity against human osteosarcoma (U2OS) cell growth^{1,2}.



Scheme 2.1. The solvent-mediated reaction producing chimaphilin (**2.10**) and **1.1** shown here side by side with the plants that are their natural sources^{23,24}.

However, the question remained whether **2.10** was the actual product of this reaction or its isomer, 2,6-dimethylnaphthalene-1,4-dione, where the methyl group is on the C6 position instead of the C7. The product could also be a mixture of the two regioisomers.

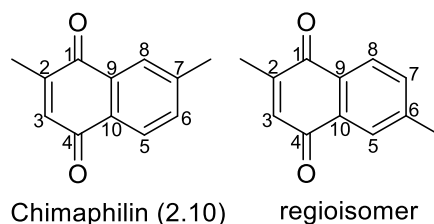


Figure 2.5. Chimaphilin and its regioisomer.

The regiochemistry of the adduct is especially important to clarify as the proposed reaction mechanism, a Diels-Alder cyclization, tends to be *para*-selective for isoprene^{25,26}. Traditional NMR analysis was inconclusive on this front; ¹³C-NMR showed doubles of the peaks, indicative of regioisomers, whereas ¹H-NMR did not show any doubles of peaks and indicated a single regioisomer. In retrospect, this must have been due to the immense structural similarity of the two regioisomers. Of course, positive structural identification and purification down to a single isomer is critical before a product can go on to biological testing, as any biological affects need to be attributable to one molecule.

2.3 REGIOCHEMISTRY DETERMINATION USING X-RAY CRYSTALLOGRAPHY

Structure elucidation via traditional ¹H- or ¹³C-NMR is inconclusive and fails to differentiate between the two isomers. The prevailing question regarding whether our lab's reaction produced true chimaphilin or its isomer prompted a turn to X-ray crystallographic technique, necessitating the crystallization of the reaction product. X-ray crystallography is a powerful structural elucidation tool that can be used to determine regiochemistry. Although single-crystal scanning is not representative of an entire sample, the diffraction pattern of chemically and enantiomerically pure samples can yield valuable structural information.

Crystals are three-dimensional structures that have long-range atomic and molecular order. To obtain chimaphilin crystals for x-ray crystallographic analysis a variety of crystallization methods were tried. Although quinones are capable of π -stacking with strong interactions²⁷, chimaphilin often failed to crystallize well, quite possibly due to the nonpolar nature of the molecule. Crystallization was attempted using either slow evaporation in the back of a fume hood or a temperature gradient from room temperature to laboratory freezer

conditions. The different crystallization attempts are summarized in Table 2.1. A chimaphilin derivative where the C2 methyl group is replaced by a phenyl group (called “phenyl chimaphilin”) was also subjected to crystallization.

Table 2.1. Attempted crystallization methods. The two entries highlighted in blue produced crystals and are discussed in more detail below.

Molecule	Method	Solvent(s)	Notes
Chimaphilin	Slow evaporation	Et ₂ O	Failed
Chimaphilin	Slow evaporation	Pentane	Failed
Chimaphilin	T gradient	THF	Dimer
Chimaphilin	T gradient	Acetone	Too small
Chimaphilin	T gradient	THF	
Chimaphilin	Slow evaporation	THF	ACN impurity? Amorphous
Chimaphilin	Slow evaporation	1:2 THF:CHCl ₃	Failed
Chimaphilin	Slow evaporation	CHCl ₃	Failed
Chimaphilin	T gradient	1:2 THF:CHCl ₃	Failed
Chimaphilin	T gradient	CHCl ₃	Fuzzy crystals
Chimaphilin	T gradient	THF	Too small
Chimaphilin	T gradient	Acetone	Failed
Chimaphilin	Slow evaporation	Isopropyl ether	Filaments, nucleation clusters
Chimaphilin	Slow evaporation	9:1 DCM:MeOH	Filaments
Chimaphilin	Slow evaporation	Toluene	Too small, nucleation clusters
Phenyl chimaphilin	T gradient	Acetone	

Slow evaporation using toluene or a 1:2 THF:CHCl₃ solvent system and a temperature gradient with THF produced small needlelike crystals that were untenable for X-Ray diffraction, which requires crystals in the range of 0.1-0.5mm. Slow evaporation with isopropyl ether or toluene did produce some noticeable nucleation clusters; these clusters are necessary for crystallization but desired in small amounts. Other attempts (such as slow evaporation with 9:1 DCM:MeOH) produced filamentous crystals which do not diffract well enough to yield crystal structures.

The Cambridge Crystallographic Data Centre’s crystal structure database, ConQuest, was used to find a crystallization method for **2.11**²⁸, which is structurally similar enough to be used as

a proxy for chimaphilin. However, the crystallization method used for **2.11** – slow evaporation using 9:1 DCM:MeOH²⁸ – failed to produce usable crystals, only resulting in hairlike filaments.

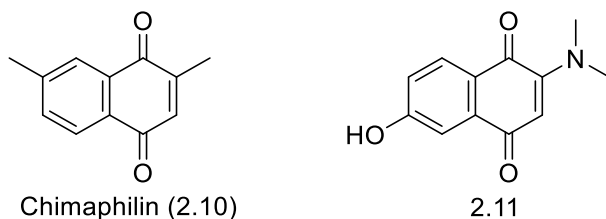


Figure 2.6. Chimaphilin and structural proxy **2.11**.

Interestingly, utilizing a temperature gradient in THF resulted in the production of a chimaphilin dimer. This dimer is likely a rare impurity that is not representative of the mixture, being taken from one of the only large crystals produced by this method. However, it does indicate the location of the methyl group in question to be on the C7 position, which is the desired regiochemistry for the molecule to constitute chimaphilin.

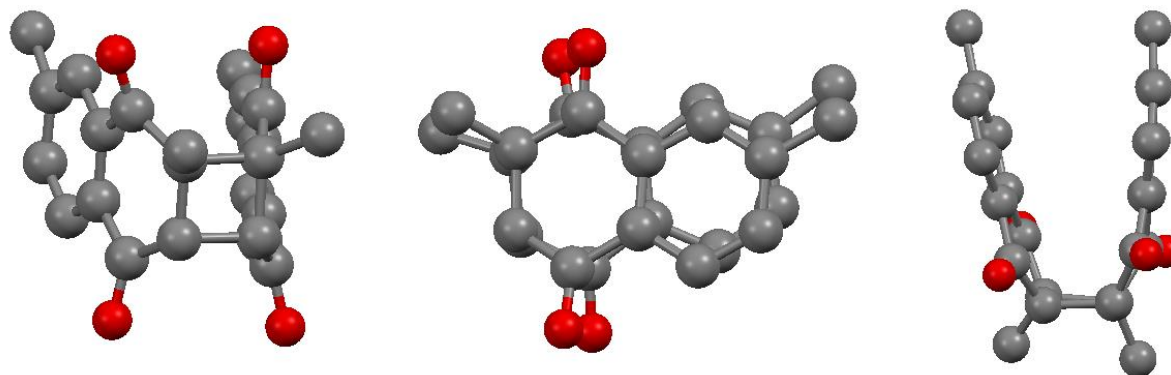
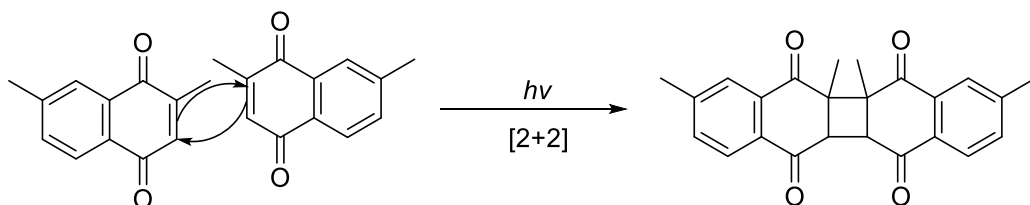


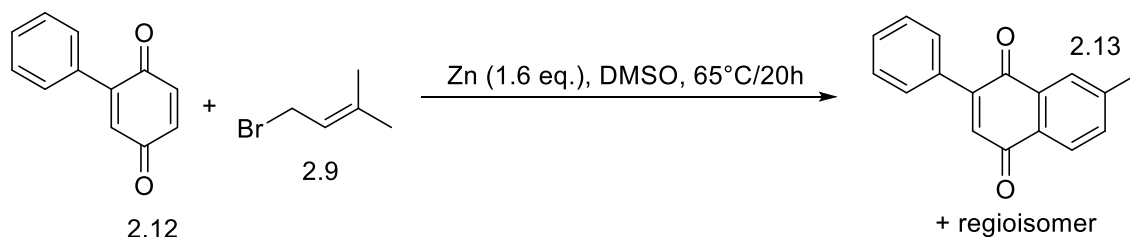
Figure 2.7. The chimaphilin dimer shown from different angles.

Presumably this dimer is produced by a photochemically induced [2+2] cycloaddition. In part, their strong electrophilic nature renders quinones somewhat reactive, so although this represents a uniqueness, it is a reasonable assumption.



Scheme 2.2. Proposed [2+2] cycloaddition reaction of chimaphilin.

The same reaction that yielded chimaphilin and its regioisomer was employed to synthesize a series of derivatives by previous members of our lab. One of these derivatives is phenyl chimaphilin (**2.13** in Scheme 2.3 below) which was more readily crystallized than chimaphilin itself by using a temperature gradient with acetone. Although these crystals were not as large as desired, they were able to diffract and were resolved as a twinned crystal – an aggregate where two crystals are growing into each other in mutual directionality. Twins are not desirable but in some cases are able to be processed structurally.



Scheme 2.3. Synthesis of phenyl chimaphilin.

Although crystallization had previously shown a peculiarity in the form of the unsuspected [2+2] dimer, the recurrence of surprise is one of those sometimes delightful, sometimes frustrating elements within laboratory procedures. Indeed, the phenyl chimaphilin crystals revealed a unique insight into the molecular structure. Though the co-crystallization of isomers is very rare, there

appeared to be not only the undesired C6-methyl isomer (predominant at ~80% abundance) but also the C7-methyl isomer (~20%).

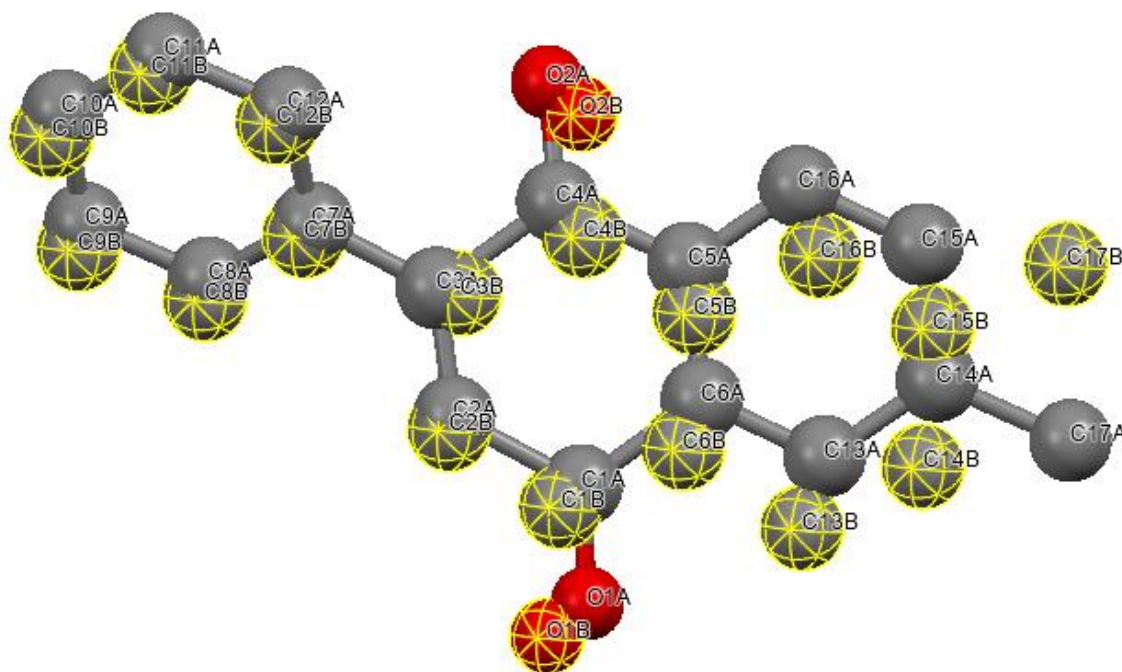


Figure 2.8. The co-crystallized isomeric structure, with the C6-methyl isomer labeled as “A” atoms and the C7-methyl isomer labeled as “B” atoms. “B” atoms have been highlighted to help show structure of the C7-methyl isomer and are somewhat disorderly in the structure due to low diffraction density.

The unit cell, or the smallest repeating volume unit of the crystal, for the isomeric crystal was found to be orthorhombic. Isomeric ratios for phenyl chimaphilin should not be taken as representative of isomeric ratios for chimaphilin, even though the same reaction method is used to synthesize both. It is possible, for instance, that the C6-methyl isomer is more predominant in the phenyl chimaphilin derivative due to steric hindrance from the bulky phenyl ring. It is also a stretch to use this information as indicative of the isomeric ratio in the entire phenyl chimaphilin reaction mixture, as the exact ratio may differ from crystal to crystal. At best, this information

positively confirms the presence of isomers in the purified phenyl chimaphilin reaction and may potentially point to steric effects upon the mechanism.

Research is ongoing to find a reliable way to crystallize chimaphilin, which has the dubious honor of being soluble in many common solvents used for crystallization, making certain methods of crystallization unattainable (for instance, liquid diffusion).

3 QUINAZOLINE-BASED SMALL MOLECULE INHIBITOR EVP4593

3.1 MOTIVATION

Although not a natural product, EVP4593 (**3.1**) is of interest as an already established MCI inhibitor, shown to have an impressive IC_{50} of 14 ± 2 nM in purified *Bos taurus* heart MCI and 25 ± 4 nM in the obligate aerobic yeast *Yarrowia lipolytica*²⁹ MCI, which are IC_{50} values comparable to DQA, a well-known MCI inhibitor³. While the effects on MCI inhibition are of primary interest to this study, EVP4593 has also been shown to have certain neuroprotective effects and has been identified as a potential Huntington's Disease therapeutic³⁰, has demonstrated powerful anthelmintic activity against parasitic worms³¹, and is an inhibitor of the NF- κ B pathway and of TNF- α production³². When tested against other mitochondrial ETC complexes, EVP4593 was also found to be selective for MCI³.

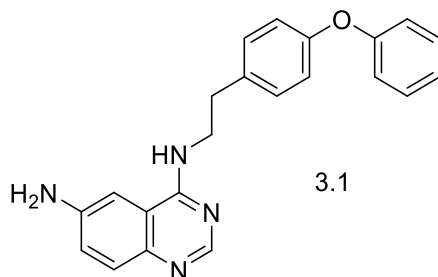


Figure 3.1. Chemical structure of EVP4593.

There are a few important structural features in EVP4593 that are believed to influence MCI inhibition. The first of note is the heterocyclic ring structure, called a quinazoline; although heterocyclics in and of themselves are denoted “an important group of biologically active compounds”³³, it is the quinazoline ring of EVP4593 in particular that is key to this research. Although a wide variety of chemical structures are reported MCI inhibitors³⁴, quinazolines and quinazoline-like structures such as EVP4593 can yield strong inhibition responses, some in the nanomolar IC₅₀ range^{3,35}. Quinazoline structures are also present in compounds displaying a host of medicinal activities, including antiviral, antibacterial, antifungal, and anticancer properties³³. According to Karan et al., “quinazoline has a very broad spectrum of pharmacological activities with minimum side effects”³³. Although EVP4593 is itself not a natural product, quinazoline structures are featured in >200 natural products³³, indicating a biological or “natural” use that makes synthetic quinazoline-based structures attractive therapeutics. From a practical standpoint, quinazoline and quinazolinone (where the quinazoline has an additional carbonyl) structures are already in use in synthetic organic chemistry³⁶, laying the foundation for quinazoline-based molecule production. For these reasons a quinazoline skeleton is an attractive starting point for MCI inhibitor design. To further illustrate the utility of the quinazoline moiety in anticancer drugs, it is of note that there are a number of approved quinazoline-based anticancer drugs on the market, including Dacomitinib (**3.2**), for non-small cell lung carcinoma, and Erlotinib (**3.3**), for several different types of cancer³³.

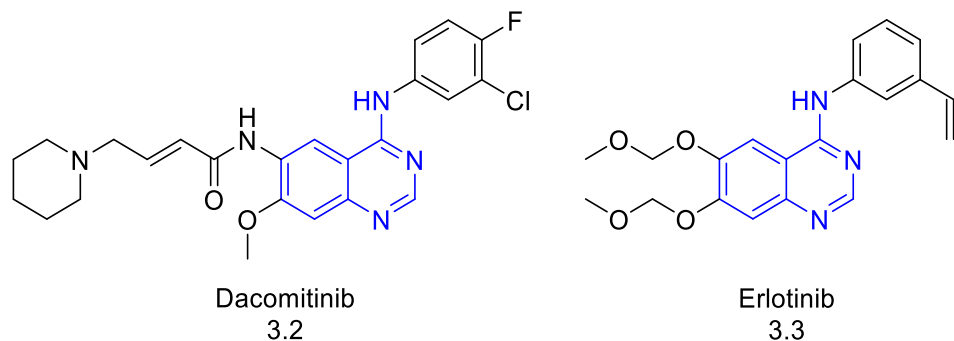


Figure 3.2. Examples of anticancer drugs with quinazoline moiety. Substructure identical to the quinazoline core of EVP4593 is shown in blue.

The phenoxyphenyl substituent in EVP4593 (Figure 3.1) increases the overall hydrophobicity of the molecule, an important consideration as any drug must be deliverable into cellular systems (requiring it to pass through a lipid bilayer). Hydrophobic concerns may be of special interest for MCI inhibitors as previous research indicates coenzyme Q10 – the natural substrate – interacts with MCI via a lipophilic pathway³.

Krishnathas et al. tested a series of similarly structured molecules to show that a C6 bromine substituent lowered inhibitory activity, indicating the importance of the C6 substituent position³. This finding is confirmed in another study that found the C6 position to be important to NF- κ B and TNF- α inhibition³²; this study will be discussed in more detail later.

Lastly, a trifluoromethyl (CF₃) group was substituted for H on the *para* position of the phenoxy ring system. Fluorine itself is a component in most of the 2020 FDA-approved drugs and its introduction can result in dramatic changes in biological activity³⁷ due in part to the intense electron-withdrawing effect of the fluorine³⁸. Metabolically speaking, the C-F bond is particularly strong³⁸, which helps to prevent drug excretion until it has had enough time to cause the desired biological effect. Some examples of approved drugs containing trifluoromethyl

groups include the anticancer agents Selinexor (**3.4**), Apalutamide (**3.5**) – specific against prostate cancer, and Alpelisib (**3.6**) – specific against breast cancer³⁷.

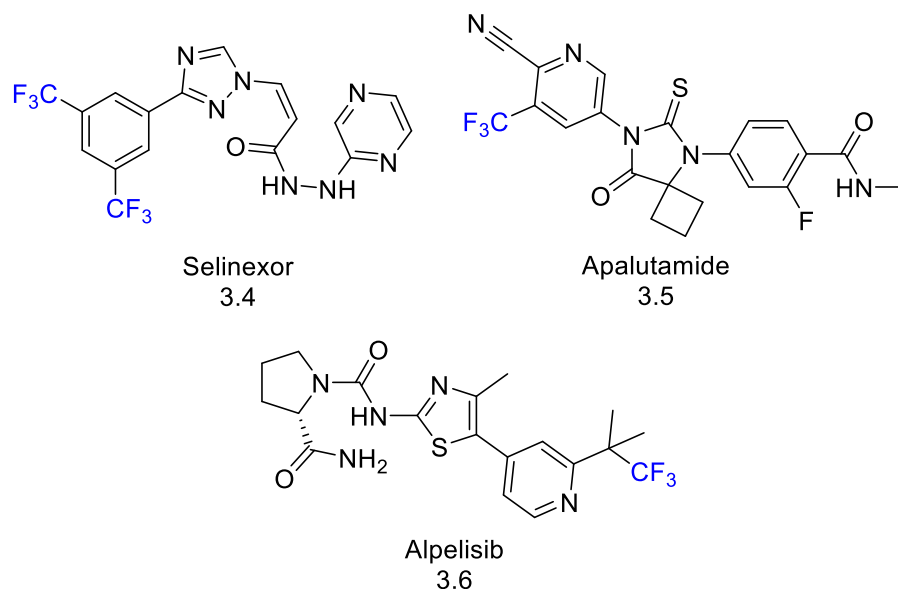
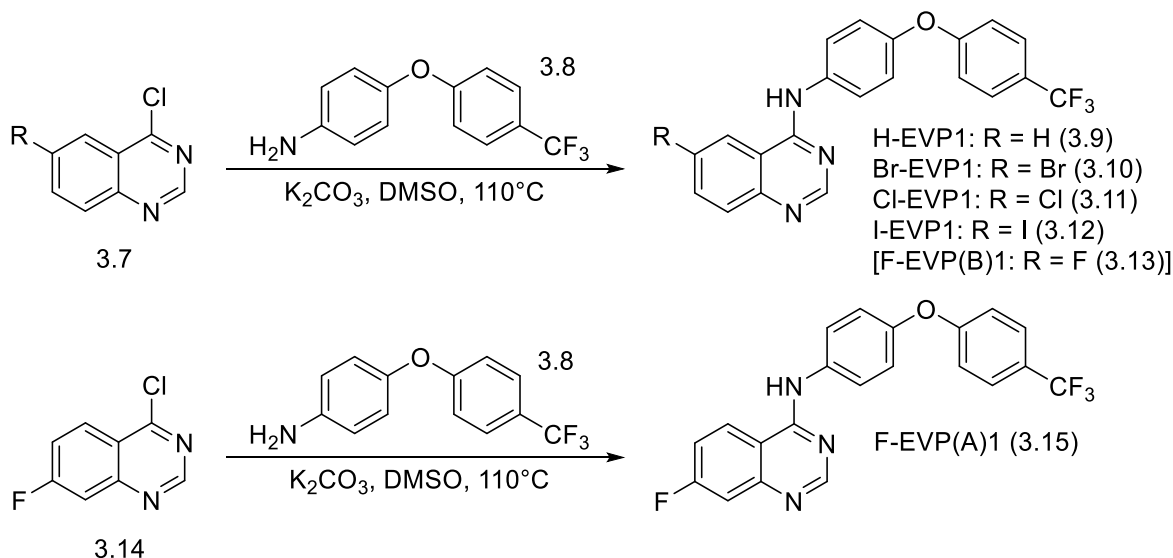


Figure 3.3. Structures of Selinexor, Apalutamide, and Alpelisib.

3.2 SYNTHESIS OF EVP4593 DERIVATIVES

The synthesis of EVP4593 derivatives mimicked a reaction originally laid out by Lee et al.³⁹, with slight modifications in terms of starting materials and occasionally in purification. All are relatively quick and easy one-step syntheses and, with the exception of H-EVP1, are novel molecules that have never been synthesized before. The generalized reaction scheme is shown below.



Scheme 3.1. Generalized reaction sequence for Series 1 EVP4593 derivatives.

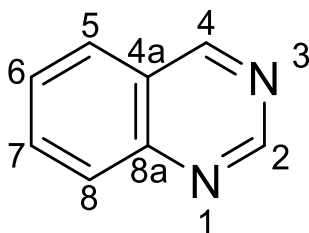


Figure 3.4. The numbered quinazoline ring.

The naming convention titles the synthesized derivatives with the elemental symbol of the C6 or C7 substituent followed by “EVP”, then the number 1 to indicate the first series of EVP4593 derivatives (additional series of derivatives characterized by alternative structural changes are part of the future research intended for this study). For example, “H-EVP1” indicates a hydrogen C6 substituent. The two fluorinated isomers are further distinguished as either (A) or (B). F-EVP(A)1, where the fluorine is on the C7 position, was merely the first to be synthesized, thus receiving the first letter of the alphabet. Of those listed, all have been successfully synthesized in the one step shown except for F-EVP(B)1, which has failed to be characterized following this

reaction sequence and thus the synthesis attempts were unsuccessful. Although unknown why the F-EVP(B)1 reaction failed, it is possible that the quinazoline starting material was decomposed by exposure to too much heat³⁶ – although this is unlikely as the same starting material remained stable in previous reactions that were under almost identical conditions. A repeated attempt yielded no product.

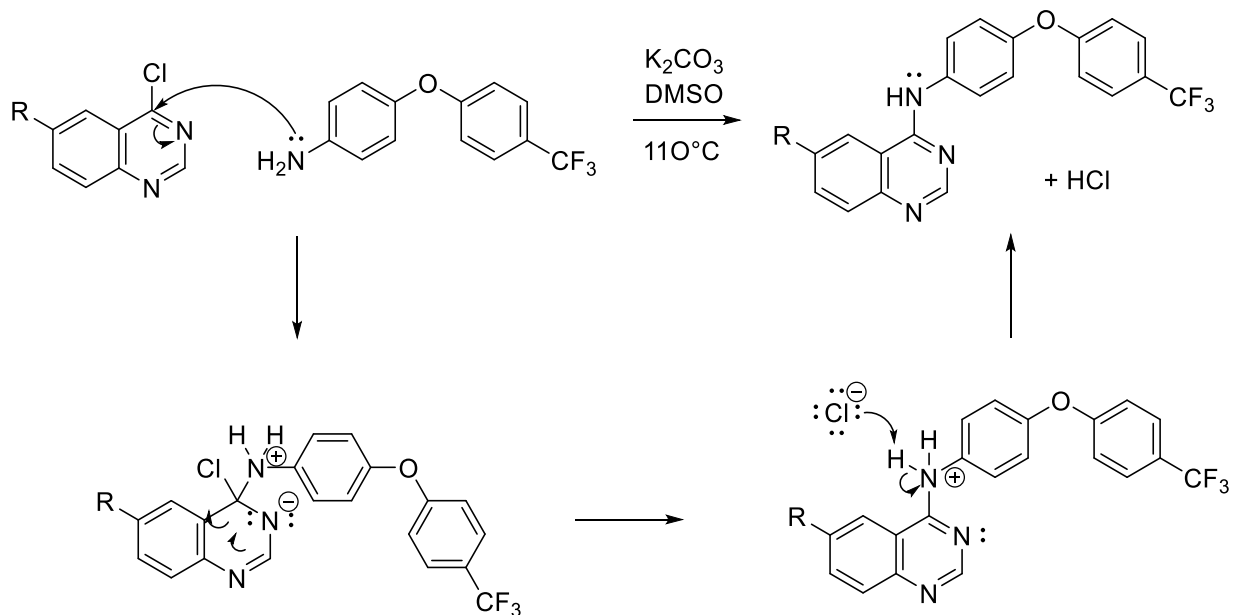
Table 3.1. Physical attributes of synthesized EVP4593 derivatives.

	State	Color	Notes
H-EVP1	Solid powder	White	Hygroscopic
Br-EVP1	Solid powder	Light brown	Hygroscopic
F-EVP(A)1	Solid powder	White	Hygroscopic
Cl-EVP1	Solid powder	Shiny yellow	Hygroscopic
I-EVP1	Solid powder	Shiny gold brown	Hygroscopic

This derivatization represents a small-scale Structure-Activity Relationship (SAR) study. In SAR studies, derivatives share a common molecular framework and differ only in isolated and distinct structural changes. SAR studies are powerful not only in that they allow for a highly creative, functional approach to drug design, but they can also be used to determine the effects of specific chemical moieties: for example, if switching out a particular alkyl chain for another (keeping the molecule otherwise the same) results in a unique biological activity, the new activity can be more or less accredited to the alkyl chain substitution. For Series 1 EVP4593 derivatives, only the C6 substituent (either a hydrogen or a halogen) was changed.

The reaction for the formation of our EVP4593 derivatives constitutes a nucleophilic aromatic substitution (S_NAr) reaction where the chlorine on the quinazoline starting material acts as a leaving group that is replaced by the nucleophilic aryl amine reactant. The halogen located on the quinazoline's C6 or C7 – either F, Cl, Br, or I on our derivatives – does not act as a leaving group and therefore a substitution at those positions does not compete with this reaction. This is because the C4 position (where the chlorine leaving group is attached) is part of a

heterocyclic structure and thus far more electron-deficient, providing a preferred electrophilic site for the amine nucleophile. Thus, this particular S_NAr reaction can be considered regioselective. The product is more electron-rich than either of the two starting materials, which slows down a second nucleophilic substitution⁴⁰, preventing the trialkylation of the amine nucleophile.



Scheme 3.2. EVP4593 derivative reaction mechanism. The “R” group represents either the H, F, Cl, Br, or I substituents.

S_NAr is “one of the preferred methods to derivatize arenes” because it is easy, cheap, and avoids the transition metals used in other methods⁴⁰. Nitrogen nucleophiles in particular are commonly used⁴⁰ and, in some cases, can be used with selectivity and high yield.

3.3 FUTURE EVP4593 DERIVATIVE SYNTHESSES

Future synthetic prospects for EVP4593 SAR analysis involve changing up other moieties on the basic EVP4593 structure, including the identity of the substituent on the C7 carbon, the number of carbons in the linker chain between the quinazoline ring and the phenoxy segment, and the

presence or absence of the trifluoromethyl group. Although investigating EVP4593 as an NF- κ B pathway and TNF- α inhibitor, Tobe et al. discovered several chemical moieties that played a role in inhibition: the number of carbons in the linker chain, the location of the nitrogens within the quinazoline base at positions 1 and 3 (as in EVP4593), and the substituent at C6³². As MCI inhibition is different from either NF- κ B or TNF- α inhibition (being a different enzyme and pathway altogether), these identified moieties serve as guidelines rather than rules for this SAR study. The possibilities for derivatization extend beyond the three potential series listed in Table 3.2 and are also variable depending on the biological results obtained.

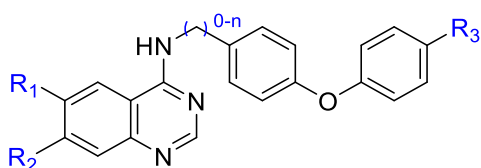


Figure 3.5. Basic chemical skeleton of future planned derivatives. Locations of specific structural changes highlighted in blue.

Table 3.2. Series 1-3 of EVP4593 SAR analysis. Compounds that have been fully synthesized are highlighted in blue.

	R ₁	R ₂	R ₃	#C		R ₁	R ₂	R ₃	#C		R ₁	R ₂	R ₃	#C
Series 1	H	H	CF ₃	0	Series 2	H	H	CF ₃	0	Series 3	H	H	CF ₃	0
	F	H	CF ₃	0		H	F	CF ₃	0		H	H	CF ₃	1
	Br	H	CF ₃	0		H	Br	CF ₃	0		H	H	CF ₃	2
	Cl	H	CF ₃	0		H	Cl	CF ₃	0		NH ₂	H	CF ₃	2
	I	H	CF ₃	0		H	I	CF ₃	0		H	H	CF ₃	3

4 BIOLOGICAL TESTING OF EVP4593 AND DERIVATIVES

4.1 IN VIVO TESTING

This part was performed in collaboration with Professor Kerscher's Research Group in the W&M Biology Department.

One important aspect of designing potential drugs is the mechanistic understanding of how the drug interacts with the target enzyme. In order to explore enzymatic interactions, EVP4593 was tested *in vivo* against a genetic knockout library of >5100 *Saccharomyces cerevisiae* (*S. cerevisiae*) – a species of yeast – strains. This is done to pinpoint any proteins or metabolic pathways that EVP4593 targets or interacts with; analysis of the gene ontology of a sensitive *S. cerevisiae* mutant allows for the inference of which gene products are key to EVP4593's biological processing. For example, a mutant that lacks the proteins required for anaerobic metabolism is forced to produce ATP via aerobic methods (that is, via the ETC); if the mutant's growth is inhibited by EVP4593, then it can be reasonably inferred that EVP4593 interferes with aerobic metabolism (since the yeast is unable to produce energy via anaerobic metabolism).

The growth of wild type (WT) *S. cerevisiae* was shown to be greatly impaired after being treated with EVP4593. The WT was grown in standard YEP G/E media and then inoculated at different concentrations of EVP4593.

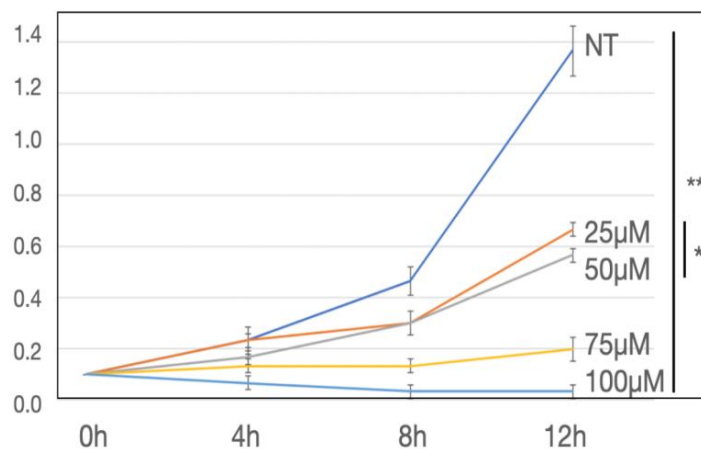


Figure 4.1. Time of sampling v. WT *S. cerevisiae* growth at given EVP4593 concentrations. After 12 hours a significant difference ($p < 0.01$) was seen for all tested EVP4593 concentrations. “NT” indicates no treatment (control).

Fluorescent microscopy was used to visualize possible fragmentation in mitochondria stained with su9-RFP (red fluorescent protein) of both untreated *pdr5Δ* and EVP4593-inoculated (100 μM) *pdr5Δ*. Microscopy revealed EVP4593-treated mitochondrial fragmentation. Krishnathas et al. indicated generation of reactive oxygen species (ROS) from EVP4593 inhibition of MCI³; if so, it is possible that ROS damage mitochondrial DNA and cause dysfunction.

EVP4593 treatment was found to cause other significant morphological changes in *S. cerevisiae* cells, notably an increase in *pdr5Δ* cell diameter and an unusual bend in the septin ring (a specific part of yeast cells). The reason behind these effects is not yet known but may have to do with cell cycle delays.

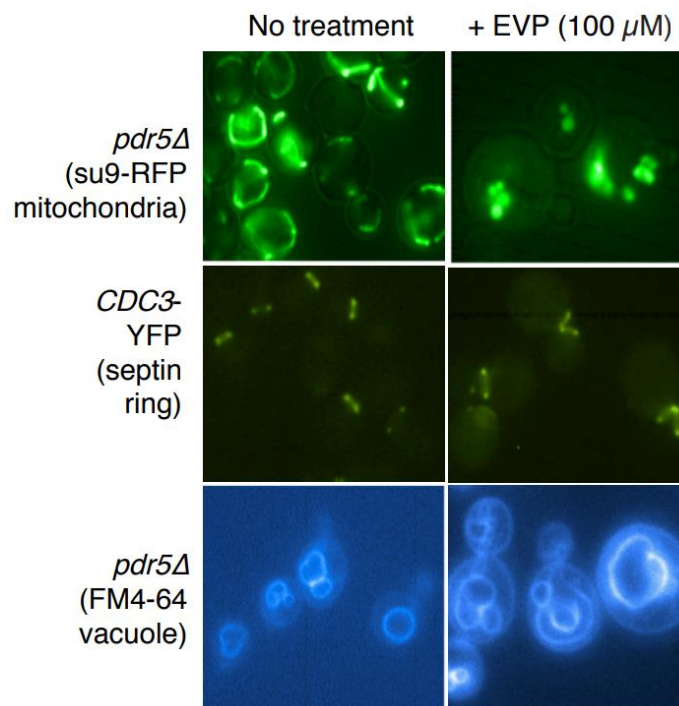


Figure 4.2. Electron microscopy images of *pdr5Δ* cells, both untreated (left) and EVP4593-treated (right). Mitochondria are tagged with a red fluorescent protein (su9-RFP), septin rings are tagged with yellow fluorescent protein (YFP), and vacuoles are visualized using FM4-64 staining.

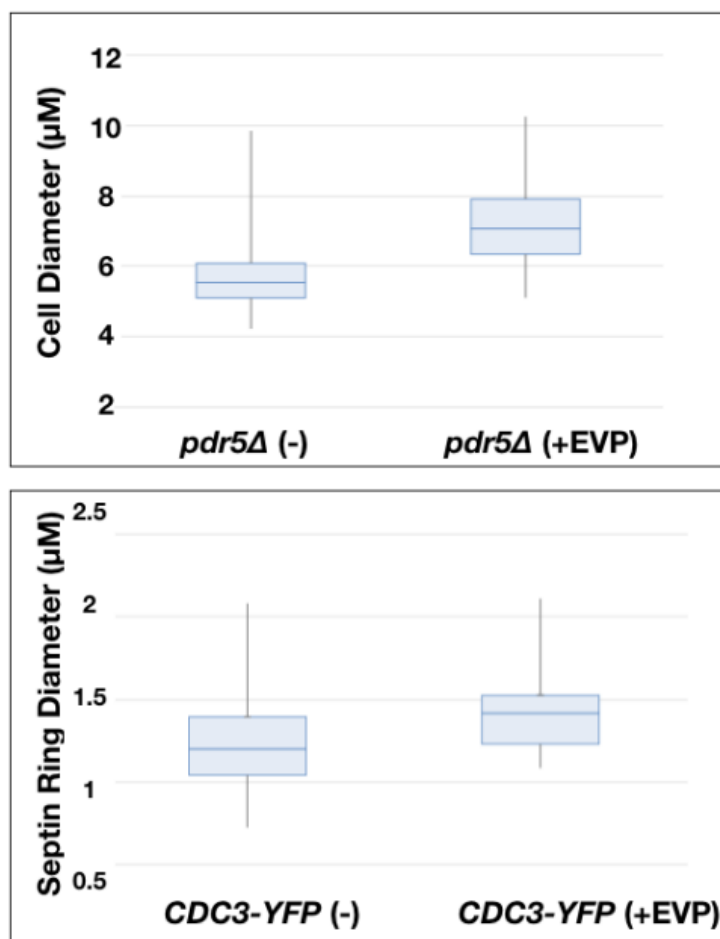


Figure 4.3. Box and whisker plots showing the diameter of *pdr5Δ* cells (top) and septin rings (bottom). Treatment lasted for 6 hours. A single-factor ANOVA test was used ($p=0.001^*$), indicating statistically significant effects on both cell diameter and septin ring diameter.

A screen of the yeast knockout collection was used to identify EVP4593-sensitive mutants for further testing. After initial screening, a follow-up serial dilution spotting assay was performed to not only confirm that EVP4593 was consistently toxic to sensitive strains but also to determine concentration-dependent toxicity. From this secondary screen, ~20 strains were identified as consistently and effectively sensitive to EVP4593.

The photographs in Figures 4.1-4.3 show the growth of yeast colonies (as gray spots) in either control or inoculated media (indicated by the column). The more toxic a compound is, the

less the yeast will grow, and the more faded the spot will appear. Side by side spots in the same photograph show summary dilutions (for which some fading is expected).

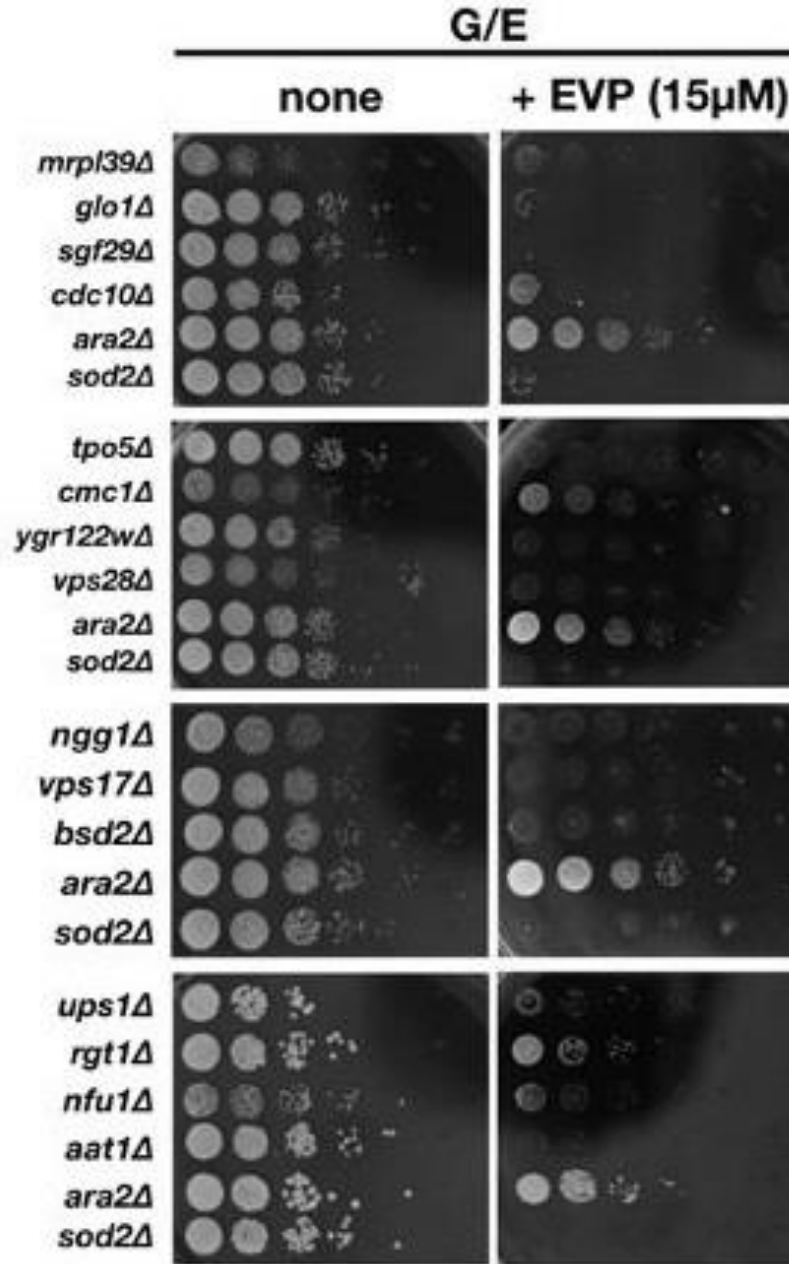


Figure 4.1. A serial dilution spotting assay showing the strains most sensitive to EVP4593. Strain *ara2Δ* is a positive control, while *sod2Δ* is a negative control. Each consecutive spot represents a ten-fold dilution.

These 20 EVP4593 sensitive mutants were grown on a non-fermentable carbon source alongside control strains *ara2Δ* (EVP4593-resistant) and *sod2Δ* (benchmark sensitive) and then serially diluted before spotting on control (YEP G/E) and experimental (YEP G/E + EVP4593, YEP G/E + Br-EVP1, YEP G/E + I-EVP1, YEP G/E + H-EVP1, YEP G/E + F-EVP(A)1) and growing for 3-5 days at 30°C. EVP4593 was tested directly against Br-EVP1, while the remaining derivatives (H-EVP1, I-EVP1, F-EVP(A)1) were tested directly against each other.

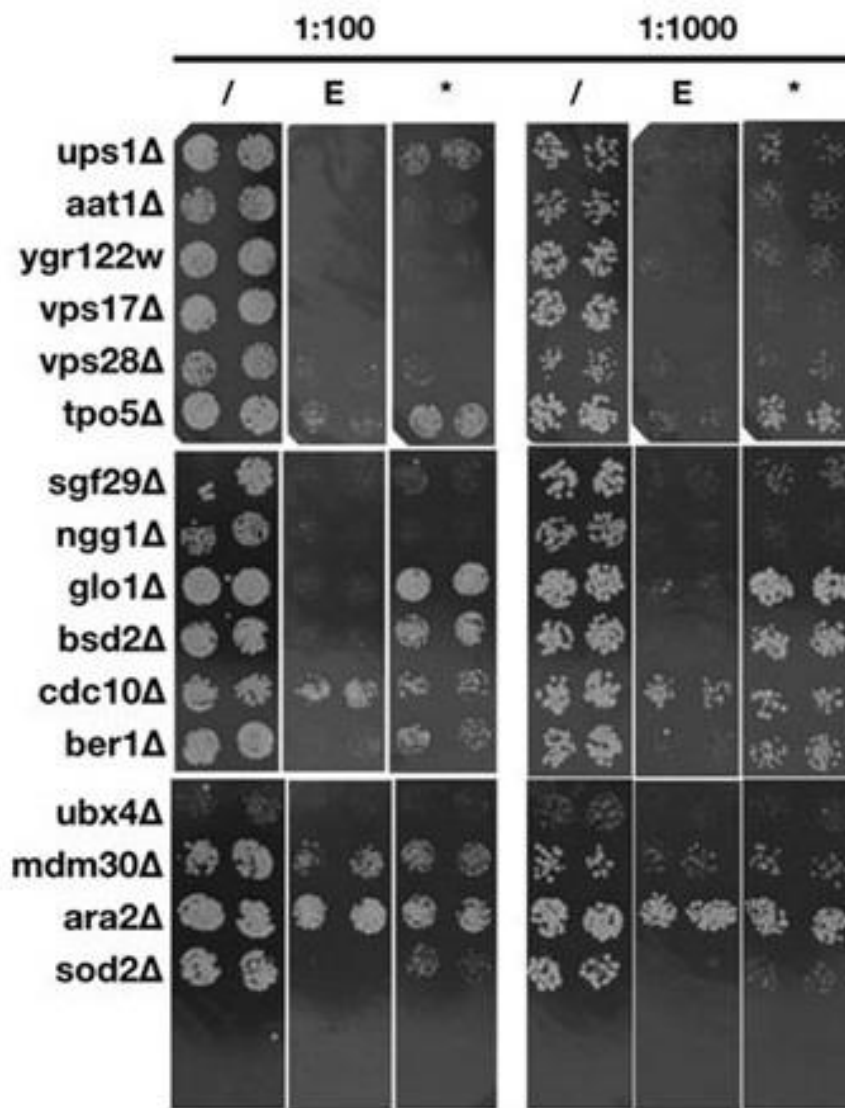


Figure 4.2. EVP4593 tested against Br-EVP1. “/” indicates the standard YEP G/E media, “E” indicates treatment with EVP4593 (15 μ M), and “*” indicates treatment with Br-EVP1 (15 μ M).

From Figure 4.2, it is seen that EVP4593 is generally more toxic than Br-EVP1, although Br-EVP1 is still fairly harmful to certain yeast strains, such as *vps17Δ* (related to vesicle transport) and *ngg1Δ* (related to transcription activation).

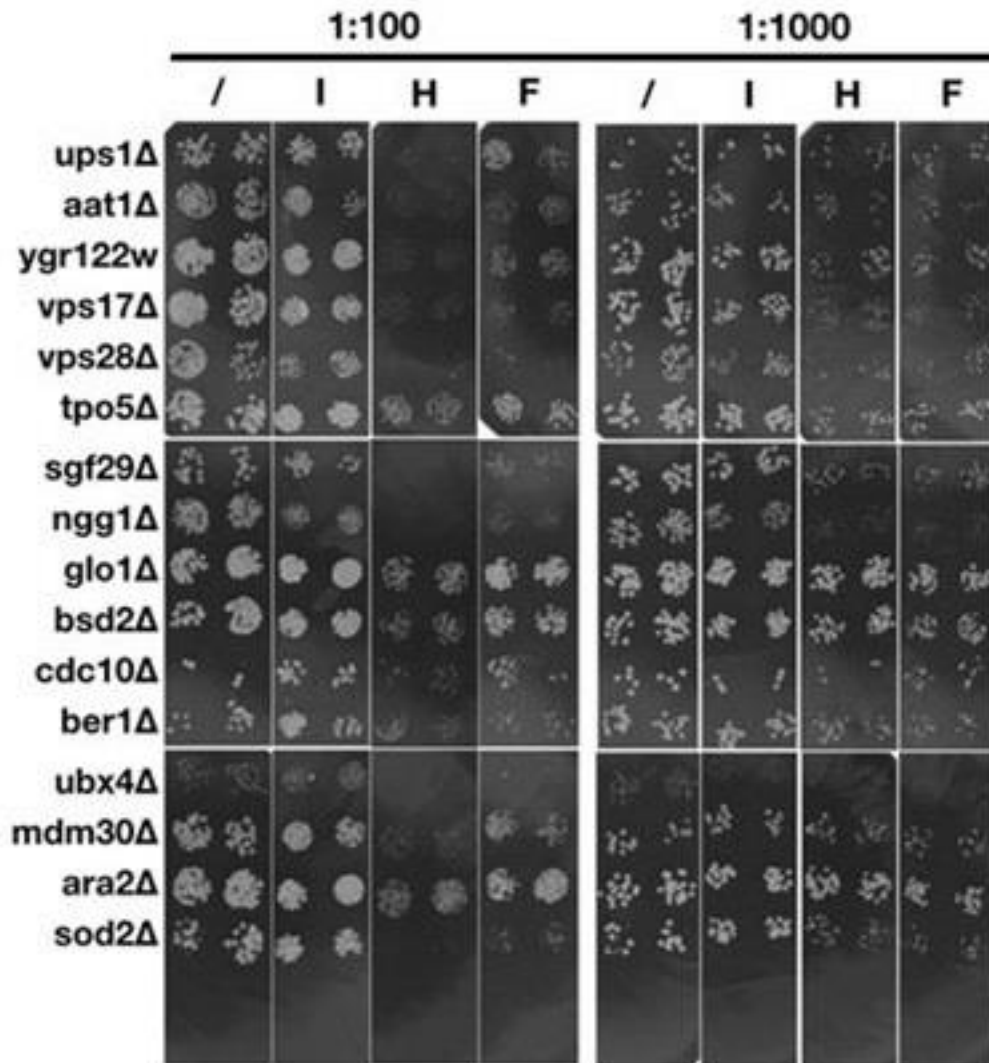


Figure 4.3. I-EVP1, H-EVP1, and F-EVP(A)1 tested against each other. “/” indicates the standard YEP G/E media, “I” indicates treatment with I-EVP1 (15 μ M), “H” indicates treatment with H-EVP1 (15 μ M), and “F” indicates treatment with F-EVP1 (15 μ M).

The most potent derivative appears to be H-EVP1, which even impacted the EVP4593-resistant strain *ara2Δ*. However, I-EVP1 was hardly effective, with F-EVP(A)1 being only slightly more potent. The weak effect of these halogenated EVP4593 derivatives mirrors that of Br-EVP1, indicating that the somewhat bulky halogen substituent could prevent active site interaction (steric effects) or membrane crossing (polarity effect). When listed with F, Br, and I, EVP4593's amine group is of moderate polarity, so polar effects are unlikely to be the sole reason behind differences in EVP4593 derivative activity.

The breakdown of the functional analysis for each sensitive strain was assessed using gene ontology (GO) analysis (pantherDB.org). The PANTHER classification system is built upon 82 complete genomes and classifies genes by function⁴¹.

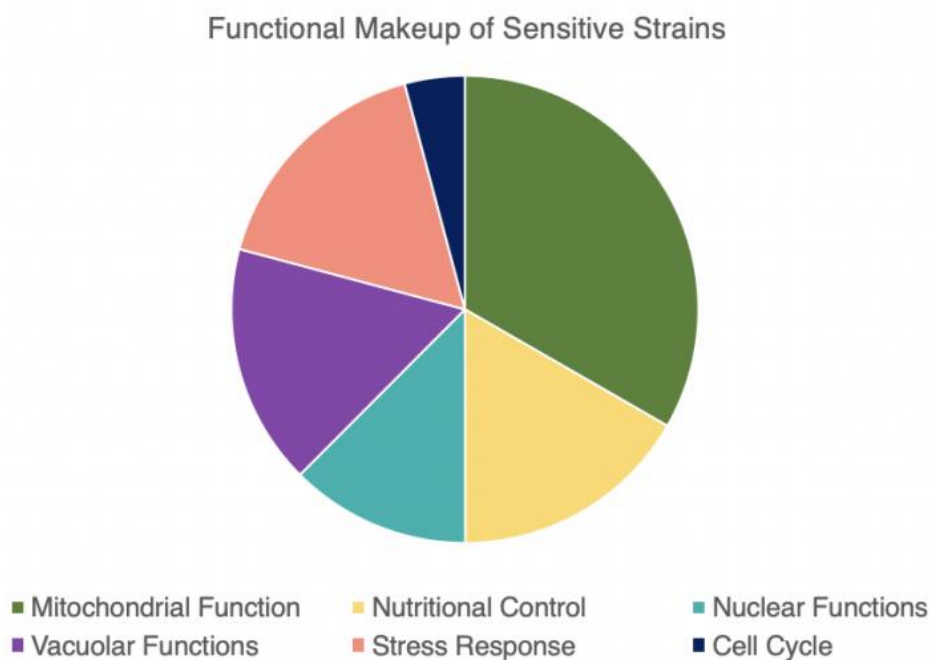


Figure 4.4. Frequency of ~20 sensitive mutant phenotypic associations.

Of the mutants' phenotypic associations, the largest section was related to mitochondrial function – a promising result since the proposed mode of action for EVP4593 and derivatives is

MCI inhibition. For example, sensitive strain *aat1* Δ lacks the gene coding for a mitochondrial-localized transferase that is involved in aspartate and asparagine biosynthesis. Interestingly, some sensitive strains had mutations related to Golgi transport or vesicle targeting, which could prevent cellular detoxification by making the cell unable to shuttle toxic materials outside of itself.

4.2 IN VITRO TESTING

This part was performed in collaboration with Professor Friedrich's Research Group at the University of Hohenheim in Germany.

Oxidases are enzymes that catalyze oxidation-reduction reactions within cells. H-EVP1 and Br-EVP1 were tested against different oxidases either in membrane (specifically the type BL21* Δ cyo) or isolated from the membrane of bacteria *Escherichia coli* (*E. coli*). Although *E. coli* do not have mitochondria, they do produce ATP via oxidative phosphorylation⁴² and the oxidases tested *in vitro* are used as bacterial analogs of eukaryotic MCI. H-EVP1 showed selectivity for dNADH oxidase, which is interesting to note as dNADH is a substrate that is specific to MCI.

In-membrane NADH, succinate, and dNADH oxidases, and isolated *bd*-I oxidase, were tested against H-EVP1. In-membrane NADH and succinate oxidases, and isolated *bd*-I and *bd*-II oxidases, were tested against Br-EVP1.

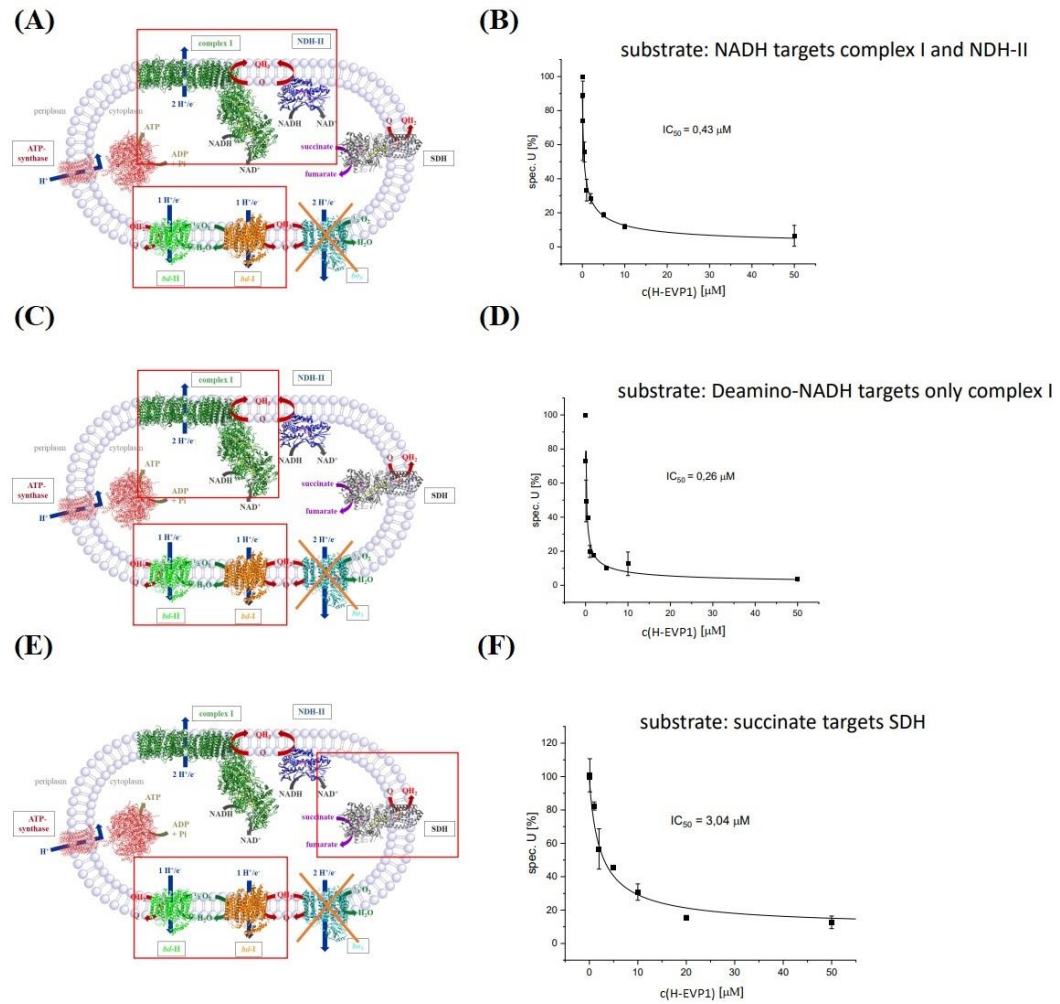


Figure 4.5. Results from treating various in-membrane oxidases with H-EVP1. (A-B) Image of a cell with complexes I, NDH-II, *bd*-I, and *bd*-II boxed; IC₅₀ plot for H-EVP1 against *E. coli* NADH oxidase. (C-D) Image of cell with complexes I, *bd*-I, and *bd*-II boxed; IC₅₀ plot for H-EVP1 against *E. coli* dNADH oxidase. (E-F) Image of cell with succinate dehydrogenase (SDH) and complexes *bd*-I and *bd*-II boxed; IC₅₀ plot for H-EVP1 against *E. coli* succinate oxidase.

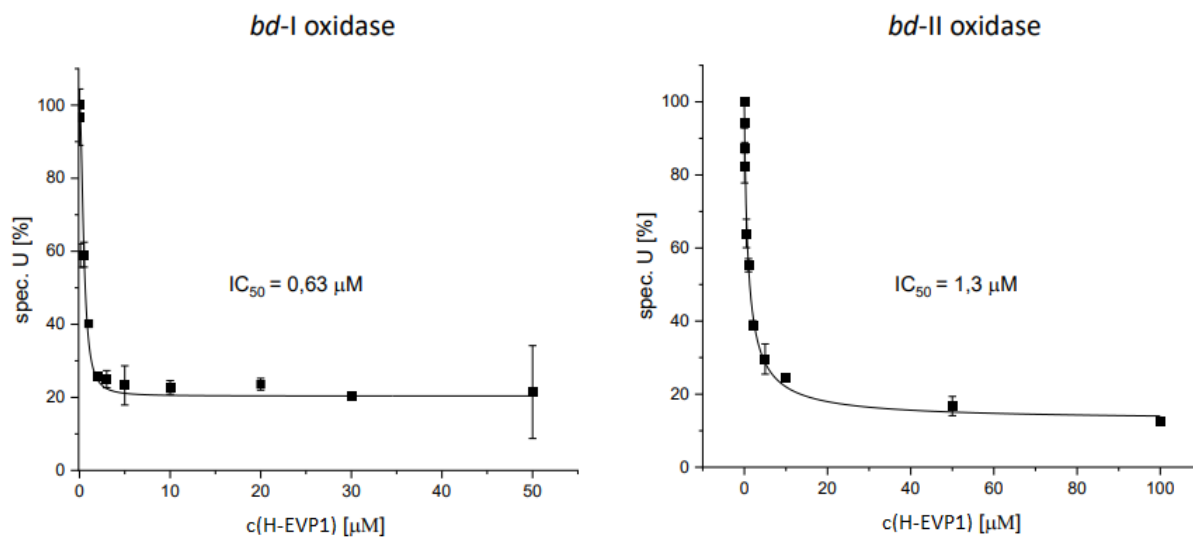


Figure 4.6. Results from treating isolated *bd-I* and *bd-II* oxidases with H-EVP1.

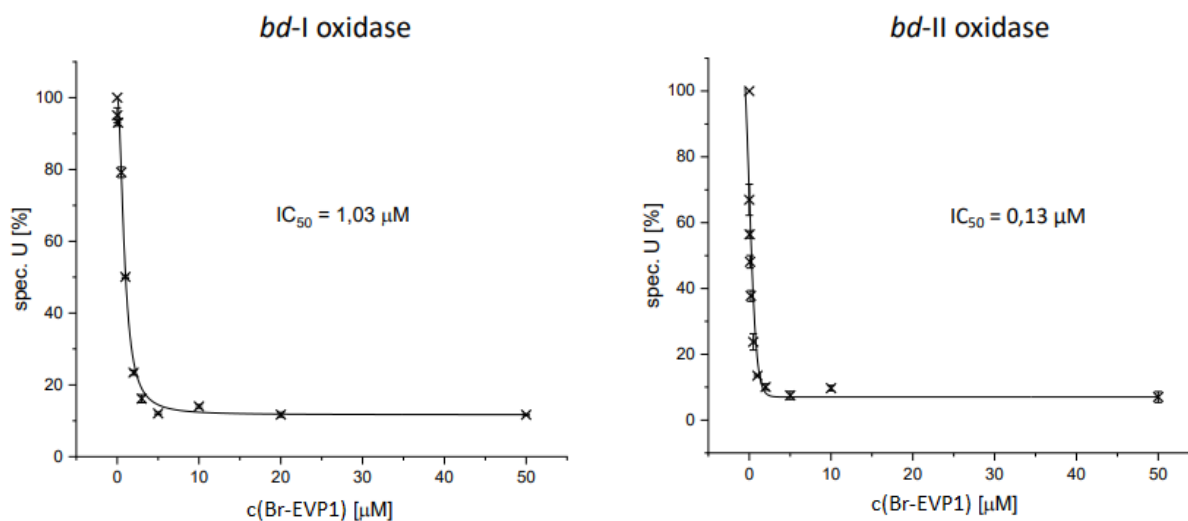


Figure 4.7. Results from treating isolated *bd-I* and *bd-II* oxidases with Br-EVP1.

Table 4.1. Oxidase IC_{50} values tested against H-EVP1 and Br-EVP1.

		H-EVP1 IC_{50} (μM)	Br-EVP1 IC_{50} (μM)
<i>E. coli</i> membranes	NADH oxidase	0.43	No effect
	Succinate oxidase	3.1	No effect
	dNADH oxidase	0.26	--
Isolated	<i>bd-I</i> oxidase	0.63	1.0
	<i>bd-II</i> oxidase	1.3	0.13

The IC₅₀ values for H-EVP1 indicated that it was specific for MCI. The in-membrane oxidases tested against Br-EVP1 showed no inhibitory effect at all, which is perhaps indicative that Br-EVP1 is unable to cross the membrane to bind oxidase active sites. This latter idea is consistent with *in vivo* testing results that showed lower inhibitory effects of the halogenated EVP4593 derivatives.

4.3 SIGNIFICANCE AND FUTURE PROSPECTS

Together, *in vivo* and *in vitro* biological testing suggest that H-EVP1 is a potent and specific inhibitor of MCI. Halogenated derivatives did not appear to be particularly effective in general, perhaps because of difficulty with membrane crossing.

The future of the EVP4593 SAR study should focus on isolating those moieties that are most effective on MCI inhibition and on further derivatization to reflect those findings. The ideal EVP4593-based inhibitor should be both specific to and a potent inhibitor of MCI, without causing any deleterious side effects that would cause excessive harm to other parts of the cell.

5 SUPPLEMENTAL INFORMATION

5.1 Instrumentation and General Synthetic Procedures

The chimaphilin dimer was crystallized using a temperature gradient in THF. Phenyl chimaphilin was crystallized using a temperature gradient in acetone. Crystals were mounted on glass fibers. All measurements were made using graphite-monochromated Mo Ka or multi-layer optics-monochromated Cu Ka radiation on a Bruker-AXS DUO three-circle diffractometer, equipped with an Apex II CCD detector. Initial space group determination was based on a matrix consisting of 36 frames (Mo) or 90 frames (Cu). Diffraction data were collected at 100 K. The

data were reduced using SAINT+ and empirical absorption correction applied using SADABS. Structures were solved using intrinsic phasing. Least-squares refinement for all structures was carried out on F^2 . All non-hydrogen atoms were refined anisotropically. Hydrogen atoms were placed in riding positions and refined isotropically. Structure solution, refinement, and the calculation of derived results were performed using the SHELXTL package of computer programs⁴³ and ShelXle⁴⁴.

Commercially available reagents were purchased from Alfa Aesar, Millipore Sigma, and Acros Organics. Reaction setup included dry glassware, magnetic stir plate and bar, a thermometer to monitor temperature, and a heating mantle. Reactions were monitored by Thin-layer chromatography using Analtech Silica gel HLF UV254. TLC plates were visualized using a UV lamp. Flash chromatography was done with Acros Organics 0.035-0.070mm, 60Å silica gel.

Proton and Carbon NMR data were taken on an Agilent VnmrJ4 spectrometer and recorded in ppm against the NMR solvent or TMS as the internal standard. GC/MS data were obtained using Agilent 6890N/5973 GCMS system.

5.2 Procedure for Synthesis of 3.9 (H-EVP1)

4-Chloroquinazoline (CAS: 5190-68-1, 164 mg, 0.987 mmol), 4-(4-(trifluoromethyl)phenoxy)aniline (CAS: 57478-19-0, 256 mg, 0.987 mmol), and potassium carbonate (135 mg, 0.987 mmol) were dissolved in 7 mL of DMSO. The reaction was refluxed at 110°C for 21 h. The reaction mixture was concentrated *in vacuo*, dissolved in DCM, and washed with 5% acetic acid solution (2x), water (1x), and brine (1x) and dried over sodium sulfate (Na_2SO_4). The organic layer was concentrated *in vacuo* to yield 0.381 g crude product. Crude material was purified via silica gel flash chromatography using a 1:1 EA:DCM solvent system to yield 281 mg of N-(4-(4-(trifluoromethyl)phenoxy)phenyl)quinazolin-4-amine (H-EVP1). White

solid. Molecular weight: 381.36 g/mol. The hygroscopic purified product was oven dried at 110°C overnight to evaporate water molecules. Melting point range: 155.9-187.5°C.

5.3 Procedure for Synthesis of 3.10 (Br-EVP1)

6-Bromo-4-chloroquinazoline (CAS: 38267-96-8, 477 mg, 1.97 mmol), 4-(4-(trifluoromethyl)phenoxy)aniline (CAS: 57478-19-0, 502 mg, 1.97 mmol), and potassium carbonate (265 mg, 1.97 mmol) were dissolved in 7 mL of DMSO. The reaction was refluxed at 110°C for ~31 h. The reaction mixture was washed with 5% acetic acid solution (2x), water (1x), and brine (1x) and the organic layer concentrated *in vacuo*. Crude material was purified via silica gel flash chromatography using a 1:1 EA:DCM solvent system to yield 409 mg (45%) of N-(4-(4-(trifluoromethyl)phenoxy)phenyl)quinazolin-4-amine (Br-EVP1). Brown solid. Molecular weight: 460.25g/mol. The hygroscopic purified product was oven dried at 110°C for ~2 h 40 min, leaving ~1.47 H₂O molecules/product molecule. Melting point range: 206.7-207.7°C.

5.4 Procedure for Synthesis of 3.15 (F-EVP(A)1)

4-Chloro-7-fluoroquinazoline (CAS: 16499-62-0, 367 mg, 1.97 mmol), 4-(4-(trifluoromethyl)phenoxy)aniline (CAS: 57478-19-0, 497 mg, 1.97 mmol), and potassium carbonate (274 mg, 1.97 mmol) were dissolved in ~7.1 mL of DMSO. The reaction was refluxed at 110°C for ~19 h. The reaction mixture was washed with 5% acetic acid solution (2x), water (1x), and brine (1x) and the organic layer concentrated *in vacuo* to yield 1.194g crude product. Crude material was purified via silica gel flash chromatography using a 1:5:1 Hex:DCM:EA solvent system to yield 598 mg (~76%) of 7-fluoro-N-(4-(4-(trifluoromethyl)phenoxy)phenyl)quinazolin-4-amine (F-EVP(A)1). White solid. Molecular weight: 399.35g/mol. The hygroscopic purified product was oven dried at 110°C overnight to evaporate water molecules. Melting point range: 198.2-198.5°C.

5.5 Procedure for Synthesis of 3.11 (Cl-EVP1)

4,6-Dichloroquinazoline (CAS: 7253-22-7, 197 mg, 0.987 mmol), 4-(4-(trifluoromethyl)phenoxy)aniline (CAS: 57478-19-0, 254 mg, 0.987 mmol), and potassium carbonate (132 mg, 0.987 mmol) were dissolved in ~5.1 mL of DMSO. The reaction was refluxed at 110°C for 22 h 20 min. The reaction mixture was washed with 5% acetic acid solution (2x), water (1x), and brine (1x) and the organic layer concentrated *in vacuo* to yield 0.849 g crude product. Crude material was purified via silica gel flash chromatography using a 1:5:1 Hex:DCM:EA solvent system to yield 65 mg of 6-chloro-N-(4-(4-(trifluoromethyl)phenoxy)phenyl)quinazolin-4-amine (Cl-EVP1). Molecular weight: 415.80g/mol. The hygroscopic purified product was oven dried at 110°C overnight to evaporate water molecules. Melting point range: 197.1-208.8°C.

5.6 Procedure for Synthesis of 3.12 (I-EVP1)

6-iodo-4-chloroquinazoline (CAS: 98556-31-1, 572 mg, 1.97 mmol), 4-(4-(trifluoromethyl)phenoxy)aniline (CAS: 57478-19-0, 499 mg, 1.97 mmol), and potassium carbonate (276 mg, 1.97 mmol) were dissolved in ~7.1 mL of DMSO. The reaction was refluxed at 110°C for 20 h 50 min. The reaction mixture was washed with 5% acetic acid solution (2x), water (1x), and brine (1x) and the organic layer concentrated *in vacuo* to yield 1.445g crude product. Crude material was purified via silica gel flash chromatography using a 1:5:1 Hex:DCM:EA solvent system to yield 727mg of 6-iodo-N-(4-(4-(trifluoromethyl)phenoxy)phenyl)quinazolin-4-amine (I-EVP1). Shiny gold-brown solid. Molecular weight: 507.25g/mol. The hygroscopic purified product was oven dried at 110°C overnight to evaporate water molecules. Melting point range: 202.2-204.5°C.

5.7 CRYSTALLOGRAPHIC INFORMATION

Table 5.1. Crystal data and structure refinement for both the chimaphilin dimer and the phenyl chimaphilin.

	Chimaphilin Dimer	Phenyl Chimaphilin
Identification code	mo_Lashley005_0m_a	cu_Lashley008_0m_4_a
Empirical formula	C ₂₄ H ₂₀ O ₄	C ₁₇ H ₁₂ O ₂
Formula weight	372.40	248.27
Temperature	100(2) K	100(2) K
Wavelength	0.71073 Å	1.54178 Å
Crystal system	Triclinic	Orthorhombic
Space group	P-1	Pbca
Unit cell dimensions	a = 7.9561(7) Å a = 71.8610(10)°. b = 10.0837(9) Å b = 78.128(2)°. c = 12.8911(12) Å g = 67.7740(10)°.	a = 12.2281(2) Å a = 90°. b = 7.38070(10) Å b = 90°. c = 27.1934(3) Å g = 90°.
Volume	905.23(14) Å ³	2454.26(6) Å ³
Z	2	8
Density (calculated)	1.366 Mg/m ³	1.344 Mg/m ³
Absorption coefficient	0.092 mm ⁻¹	0.699 mm ⁻¹
F(000)	392	1040
Crystal size	0.460 x 0.230 x 0.130 mm ³	0.050 x 0.050 x 0.022 mm ³
Theta range for data collection	1.671 to 26.018°.	3.250 to 69.959°.
Index ranges	-9<=h<=9, -12<=k<=12, -15<=l<=15	?<=h<=?, ?<=k<=?, ?<=l<=?
Reflections collected	12539	2303
Independent reflections	3556 [R(int) = 0.0240]	2303 [R(int) = ?]
Completeness to theta = 67.679°	99.9 %	99.8 %
Refinement method	Full-matrix least-squares on F ²	Full-matrix least-squares on F ²
Data / restraints / parameters	3556 / 0 / 257	2303 / 153 / 227
Goodness-of-fit on F ²	1.037	1.265
Final R indices [I>2sigma(I)]	R1 = 0.0375, wR2 = 0.1229	R1 = 0.0507, wR2 = 0.1122

R indices (all data)	R1 = 0.0464, wR2 = 0.1326	R1 = 0.0544, wR2 = 0.1137
Extinction coefficient	n/a	n/a
Largest diff. peak and hole	0.284 and -0.180 e.Å ⁻³	0.165 and -0.208 e.Å ⁻³

Chimaphilin Dimer

Table 5.2. Bond lengths [Å] and angles [°] for the chimaphilin dimer structure.

O(1)-C(1)	1.2202(15)	O(1)-C(1)-C(6)	120.86(11)	C(13)-C(14)-C(15)	115.31(10)
O(2)-C(4)	1.2171(15)	O(1)-C(1)-C(2)	119.40(11)	C(23)-C(14)-C(15)	113.49(10)
O(3)-C(13)	1.2186(15)	C(6)-C(1)-C(2)	119.74(11)	C(13)-C(14)-C(2)	112.85(10)
O(4)-C(16)	1.2236(15)	C(1)-C(2)-C(11)	108.32(10)	C(23)-C(14)-C(2)	114.45(10)
C(1)-C(6)	1.4939(18)	C(1)-C(2)-C(3)	115.82(10)	C(15)-C(14)-C(2)	88.99(9)
C(1)-C(2)	1.5217(17)	C(11)-C(2)-C(3)	114.35(10)	C(16)-C(15)-C(14)	119.24(10)
C(2)-C(11)	1.5298(18)	C(1)-C(2)-C(14)	112.67(10)	C(16)-C(15)-C(3)	113.42(10)
C(2)-C(3)	1.5443(18)	C(11)-C(2)-C(14)	115.39(10)	C(14)-C(15)-C(3)	90.22(9)
C(2)-C(14)	1.6166(17)	C(3)-C(2)-C(14)	89.55(9)	C(16)-C(15)-H(15)	110.8
C(3)-C(4)	1.5099(18)	C(4)-C(3)-C(2)	120.23(10)	C(14)-C(15)-H(15)	110.8
C(3)-C(15)	1.5876(17)	C(4)-C(3)-C(15)	116.10(11)	C(3)-C(15)-H(15)	110.8
C(3)-H(3)	1.0000	C(2)-C(3)-C(15)	90.46(9)	O(4)-C(16)-C(17)	121.89(12)
C(4)-C(5)	1.4883(18)	C(4)-C(3)-H(3)	109.5	O(4)-C(16)-C(15)	120.09(11)
C(5)-C(10)	1.4001(18)	C(2)-C(3)-H(3)	109.5	C(17)-C(16)-C(15)	117.92(11)
C(5)-C(6)	1.4019(18)	C(15)-C(3)-H(3)	109.5	C(22)-C(17)-C(18)	119.02(12)
C(6)-C(7)	1.4011(17)	O(2)-C(4)-C(5)	122.28(12)	C(22)-C(17)-C(16)	119.81(12)
C(7)-C(8)	1.3935(18)	O(2)-C(4)-C(3)	120.28(11)	C(18)-C(17)-C(16)	121.15(11)
C(7)-H(7)	0.9500	C(5)-C(4)-C(3)	117.41(11)	C(19)-C(18)-C(17)	120.09(12)
C(8)-C(9)	1.4000(19)	C(10)-C(5)-C(6)	118.99(12)	C(19)-C(18)-C(13)	118.76(11)
C(8)-C(12)	1.5092(18)	C(10)-C(5)-C(4)	119.31(12)	C(17)-C(18)-C(13)	121.15(11)
C(9)-C(10)	1.3876(19)	C(6)-C(5)-C(4)	121.70(12)	C(20)-C(19)-C(18)	120.83(12)
C(9)-H(9)	0.9500	C(7)-C(6)-C(5)	119.96(12)	C(20)-C(19)-H(19)	119.6
C(10)-H(10)	0.9500	C(7)-C(6)-C(1)	117.75(12)	C(18)-C(19)-H(19)	119.6
C(11)-H(11A)	0.9800	C(5)-C(6)-C(1)	122.28(11)	C(19)-C(20)-C(21)	118.39(12)
C(11)-H(11B)	0.9800	C(8)-C(7)-C(6)	120.98(12)	C(19)-C(20)-C(24)	120.48(13)
C(11)-H(11C)	0.9800	C(8)-C(7)-H(7)	119.5	C(21)-C(20)-C(24)	121.09(12)
C(12)-H(12A)	0.9800	C(6)-C(7)-H(7)	119.5	C(22)-C(21)-C(20)	121.44(12)

C(12)-H(12B)	0.9800	C(7)-C(8)-C(9)	118.60(12)	C(22)-C(21)-H(21)	119.3
C(12)-H(12C)	0.9800	C(7)-C(8)-C(12)	120.22(12)	C(20)-C(21)-H(21)	119.3
C(13)-C(18)	1.4958(18)	C(9)-C(8)-C(12)	121.18(12)	C(21)-C(22)-C(17)	120.08(13)
C(13)-C(14)	1.5229(17)	C(10)-C(9)-C(8)	120.92(12)	C(21)-C(22)-H(22)	120.0
C(14)-C(23)	1.5231(17)	C(10)-C(9)-H(9)	119.5	C(17)-C(22)-H(22)	120.0
C(14)-C(15)	1.5555(17)	C(8)-C(9)-H(9)	119.5	C(14)-C(23)-H(23A)	109.5
C(15)-C(16)	1.5084(17)	C(9)-C(10)-C(5)	120.55(13)	C(14)-C(23)-H(23B)	109.5
C(15)-H(15)	1.0000	C(9)-C(10)-H(10)	119.7	H(23A)-C(23)-H(23B)	109.5
C(16)-C(17)	1.4860(17)	C(5)-C(10)-H(10)	119.7	C(14)-C(23)-H(23C)	109.5
C(17)-C(22)	1.4007(18)	C(2)-C(11)-H(11A)	109.5	H(23A)-C(23)-H(23C)	109.5
C(17)-C(18)	1.4018(17)	C(2)-C(11)-H(11B)	109.5	H(23B)-C(23)-H(23C)	109.5
C(18)-C(19)	1.3968(17)	H(11A)-C(11)-H(11B)	109.5	C(20)-C(24)-H(24A)	109.5
C(19)-C(20)	1.3949(18)	C(2)-C(11)-H(11C)	109.5	C(20)-C(24)-H(24B)	109.5
C(19)-H(19)	0.9500	H(11A)-C(11)-H(11C)	109.5	H(24A)-C(24)-H(24B)	109.5
C(20)-C(21)	1.396(2)	H(11B)-C(11)-H(11C)	109.5	C(20)-C(24)-H(24C)	109.5
C(20)-C(24)	1.5127(19)	C(8)-C(12)-H(12A)	109.5	H(24A)-C(24)-H(24C)	109.5
C(21)-C(22)	1.3841(19)	C(8)-C(12)-H(12B)	109.5	H(24B)-C(24)-H(24C)	109.5
C(21)-H(21)	0.9500	H(12A)-C(12)-H(12B)	109.5		
C(22)-H(22)	0.9500	C(8)-C(12)-H(12C)	109.5		
C(23)-H(23A)	0.9800	H(12A)-C(12)-H(12C)	109.5		
C(23)-H(23B)	0.9800	H(12B)-C(12)-H(12C)	109.5		
C(23)-H(23C)	0.9800	O(3)-C(13)-C(18)	120.66(11)		
C(24)-H(24A)	0.9800	O(3)-C(13)-C(14)	121.56(11)		
C(24)-H(24B)	0.9800	C(18)-C(13)-C(14)	117.75(11)		
C(24)-H(24C)	0.9800	C(13)-C(14)-C(23)	110.39(10)		

Phenyl Chimaphilin

Table 5.3. Bond lengths [Å] and angles [°] for the phenyl chimaphilin structure.

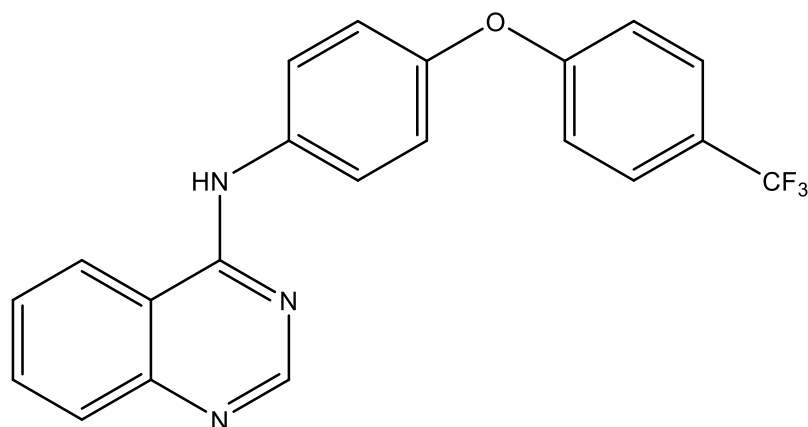
O(1A)-C(1A)	1.208(4)	C(14B)-C(15B)	1.422(14)	H(17A)-C(17A)-H(17B)	109.5
O(2A)-C(4A)	1.230(5)	C(14B)-H(14B)	0.9500	C(14A)-C(17A)-H(17C)	109.5
C(1A)-C(2A)	1.490(4)	C(15B)-C(16B)	1.371(18)	H(17A)-C(17A)-H(17C)	109.5
C(1A)-C(6A)	1.515(6)	C(15B)-C(17B)	1.513(16)	H(17B)-C(17A)-H(17C)	109.5
C(2A)-C(3A)	1.327(5)	C(16B)-H(16B)	0.9500	O(1B)-C(1B)-C(2B)	118.8(10)
C(2A)-H(2A)	0.9500	C(17B)-H(17D)	0.9800	O(1B)-C(1B)-C(6B)	121.1(10)
C(3A)-C(7A)	1.439(6)	C(17B)-H(17E)	0.9800	C(2B)-C(1B)-C(6B)	120.0

C(3A)-C(4A)	1.522(4)	C(17B)-H(17F)	0.9800	C(1B)-C(2B)-C(3B)	120.0
C(4A)-C(5A)	1.481(4)	O(1A)-C(1A)-C(2A)	121.2(4)	C(1B)-C(2B)-H(2B)	120.0
C(5A)-C(16A)	1.387(3)	O(1A)-C(1A)-C(6A)	122.8(3)	C(3B)-C(2B)-H(2B)	120.0
C(5A)-C(6A)	1.399(4)	C(2A)-C(1A)-C(6A)	116.0(3)	C(2B)-C(3B)-C(4B)	120.0
C(6A)-C(13A)	1.387(3)	C(3A)-C(2A)-C(1A)	125.6(4)	C(2B)-C(3B)-C(7B)	105.7(11)
C(7A)-C(8A)	1.391(5)	C(3A)-C(2A)-H(2A)	117.2	C(4B)-C(3B)-C(7B)	134.3(11)
C(7A)-C(12A)	1.396(5)	C(1A)-C(2A)-H(2A)	117.2	O(2B)-C(4B)-C(3B)	114.3(10)
C(8A)-C(9A)	1.383(4)	C(2A)-C(3A)-C(7A)	125.3(4)	O(2B)-C(4B)-C(5B)	125.5(10)
C(8A)-H(8A)	0.9500	C(2A)-C(3A)-C(4A)	118.2(4)	C(3B)-C(4B)-C(5B)	120.0
C(9A)-C(10A)	1.386(5)	C(7A)-C(3A)-C(4A)	116.5(4)	C(6B)-C(5B)-C(4B)	120.0
C(9A)-H(9A)	0.9500	O(2A)-C(4A)-C(5A)	119.7(3)	C(6B)-C(5B)-C(16B)	119.1(9)
C(10A)-C(11A)	1.370(6)	O(2A)-C(4A)-C(3A)	121.3(3)	C(4B)-C(5B)-C(16B)	120.9(9)
C(10A)-H(10A)	0.9500	C(5A)-C(4A)-C(3A)	119.0(3)	C(5B)-C(6B)-C(1B)	120.0
C(11A)-C(12A)	1.385(4)	C(16A)-C(5A)-C(6A)	118.6(3)	C(5B)-C(6B)-C(13B)	119.2(9)
C(11A)-H(11A)	0.9500	C(16A)-C(5A)-C(4A)	120.4(3)	C(1B)-C(6B)-C(13B)	120.8(9)
C(12A)-H(12A)	0.9500	C(6A)-C(5A)-C(4A)	121.0(2)	C(8B)-C(7B)-C(12B)	120.0
C(13A)-C(14A)	1.389(4)	C(13A)-C(6A)-C(5A)	120.8(3)	C(8B)-C(7B)-C(3B)	121.8(12)
C(13A)-H(13A)	0.9500	C(13A)-C(6A)-C(1A)	119.3(3)	C(12B)-C(7B)-C(3B)	118.2(12)
C(14A)-C(15A)	1.401(4)	C(5A)-C(6A)-C(1A)	119.9(2)	C(7B)-C(8B)-C(9B)	120.0
C(14A)-C(17A)	1.498(4)	C(8A)-C(7A)-C(12A)	117.4(3)	C(7B)-C(8B)-H(8B)	120.0
C(15A)-C(16A)	1.388(4)	C(8A)-C(7A)-C(3A)	118.5(5)	C(9B)-C(8B)-H(8B)	120.0
C(15A)-H(15A)	0.9500	C(12A)-C(7A)-C(3A)	124.1(4)	C(10B)-C(9B)-C(8B)	120.0
C(16A)-H(16A)	0.9500	C(9A)-C(8A)-C(7A)	121.8(3)	C(10B)-C(9B)-H(9B)	120.0
C(17A)-H(17A)	0.9800	C(9A)-C(8A)-H(8A)	119.1	C(8B)-C(9B)-H(9B)	120.0
C(17A)-H(17B)	0.9800	C(7A)-C(8A)-H(8A)	119.1	C(11B)-C(10B)-C(9B)	120.0
C(17A)-H(17C)	0.9800	C(8A)-C(9A)-C(10A)	119.7(3)	C(11B)-C(10B)-H(10B)	120.0
O(1B)-C(1B)	1.339(14)	C(8A)-C(9A)-H(9A)	120.1	C(9B)-C(10B)-H(10B)	120.0
O(2B)-C(4B)	1.252(17)	C(10A)-C(9A)-H(9A)	120.1	C(10B)-C(11B)-C(12B)	120.0
C(1B)-C(2B)	1.3900	C(11A)-C(10A)-C(9A)	119.4(2)	C(10B)-C(11B)-H(11B)	120.0
C(1B)-C(6B)	1.3900	C(11A)-C(10A)-H(10A)	120.3	C(12B)-C(11B)-H(11B)	120.0
C(2B)-C(3B)	1.3900	C(9A)-C(10A)-H(10A)	120.3	C(11B)-C(12B)-C(7B)	120.0
C(2B)-H(2B)	0.9500	C(10A)-C(11A)-C(12A)	121.0(4)	C(11B)-C(12B)-H(12B)	120.0
C(3B)-C(4B)	1.3900	C(10A)-C(11A)-H(11A)	119.5	C(7B)-C(12B)-H(12B)	120.0
C(3B)-C(7B)	1.703(16)	C(12A)-C(11A)-H(11A)	119.5	C(14B)-C(13B)-C(6B)	119.2(10)
C(4B)-C(5B)	1.3900	C(11A)-C(12A)-C(7A)	120.7(4)	C(14B)-C(13B)-H(13B)	120.4

C(5B)-C(6B)	1.3900	C(11A)-C(12A)-H(12A)	119.7	C(6B)-C(13B)-H(13B)	120.4
C(5B)-C(16B)	1.410(13)	C(7A)-C(12A)-H(12A)	119.7	C(13B)-C(14B)-C(15B)	120.9(11)
C(6B)-C(13B)	1.463(12)	C(6A)-C(13A)-C(14A)	120.9(3)	C(13B)-C(14B)-H(14B)	119.6
C(7B)-C(8B)	1.3900	C(6A)-C(13A)-H(13A)	119.5	C(15B)-C(14B)-H(14B)	119.6
C(7B)-C(12B)	1.3900	C(14A)-C(13A)-H(13A)	119.5	C(16B)-C(15B)-C(14B)	118.6(12)
C(8B)-C(9B)	1.3900	C(13A)-C(14A)-C(15A)	117.9(2)	C(16B)-C(15B)-C(17B)	121.8(13)
C(8B)-H(8B)	0.9500	C(13A)-C(14A)-C(17A)	121.7(3)	C(14B)-C(15B)-C(17B)	119.6(11)
C(9B)-C(10B)	1.3900	C(15A)-C(14A)-C(17A)	120.3(3)	C(15B)-C(16B)-C(5B)	123.0(11)
C(9B)-H(9B)	0.9500	C(16A)-C(15A)-C(14A)	121.5(2)	C(15B)-C(16B)-H(16B)	118.5
C(10B)-C(11B)	1.3900	C(16A)-C(15A)-H(15A)	119.3	C(5B)-C(16B)-H(16B)	118.5
C(10B)-H(10B)	0.9500	C(14A)-C(15A)-H(15A)	119.3	C(15B)-C(17B)-H(17D)	109.5
C(11B)-C(12B)	1.3900	C(15A)-C(16A)-C(5A)	120.3(3)	C(15B)-C(17B)-H(17E)	109.5
C(11B)-H(11B)	0.9500	C(15A)-C(16A)-H(16A)	119.9	H(17D)-C(17B)-H(17E)	109.5
C(12B)-H(12B)	0.9500	C(5A)-C(16A)-H(16A)	119.9	C(15B)-C(17B)-H(17F)	109.5
C(13B)-C(14B)	1.387(14)	C(14A)-C(17A)-H(17A)	109.5	H(17D)-C(17B)-H(17F)	109.5
C(13B)-H(13B)	0.9500	C(14A)-C(17A)-H(17B)	109.5	H(17E)-C(17B)-H(17F)	109.5

5.8 SPECTRAL INFORMATION

N-(4-(4-(trifluoromethyl)phenoxy)phenyl)quinazolin-4-amine (H-EVP1), 3.9



¹H-NMR (400 MHz, CDCl₃) δ ppm 8.791 (s, 1H), 7.958-7.939 (d, 1H), 7.906-7.886 (d, 1H), 7.857-7.816 (m, 1H), 7.798-7.759 (m, 2H), 7.620-7.577 (m, 3H), 7.432 (br. s, 1H), 7.151-7.077 (m, 3H).

¹³C-NMR (100 MHz, CDCl₃) δ ppm 154.909, 152.260, 134.571, ~134.571, 133.054, ~133.054, 129.199, 127.173, 127.135, 126.785, 123.644, 120.624, ~120.624, 120.077, 177.725, ~177.725, 114.970.

EI-MS: m/z 381.1 [M^+] found at peak (retention time) from 27.691-29.548 min.

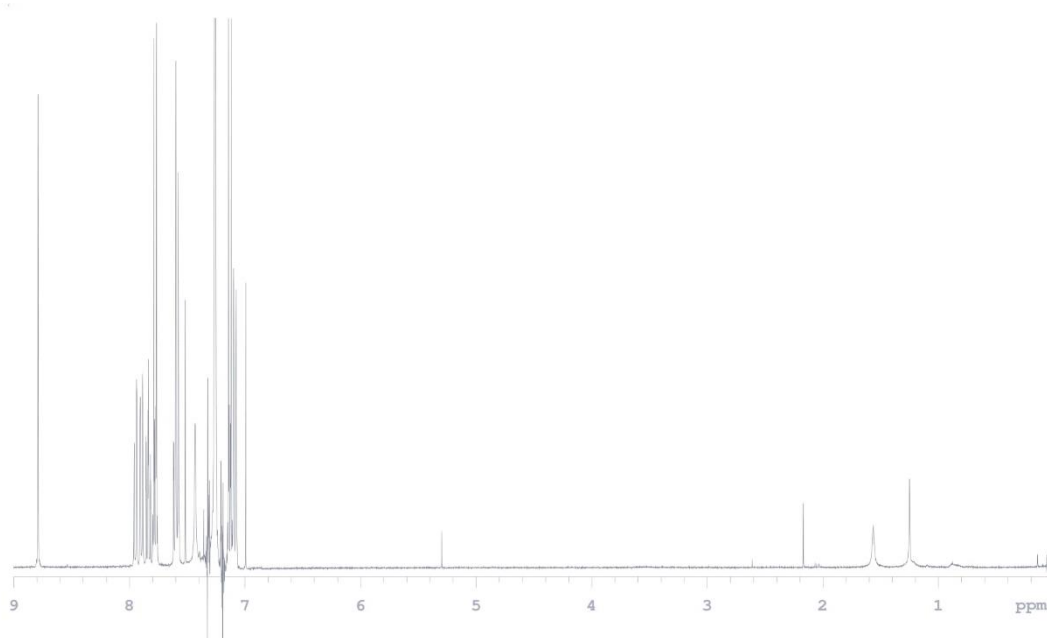


Figure 5.1. ^1H -NMR spectrum of H-EVP1.

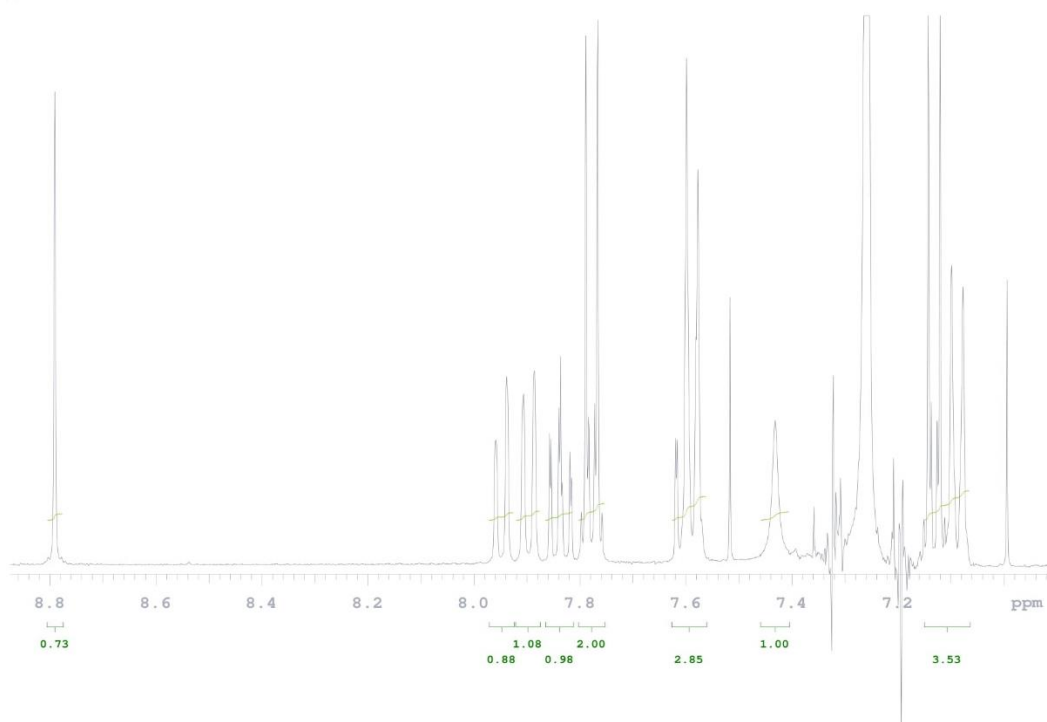


Figure 5.2. Zoom of ^1H -NMR aromatic region of H-EVP1.

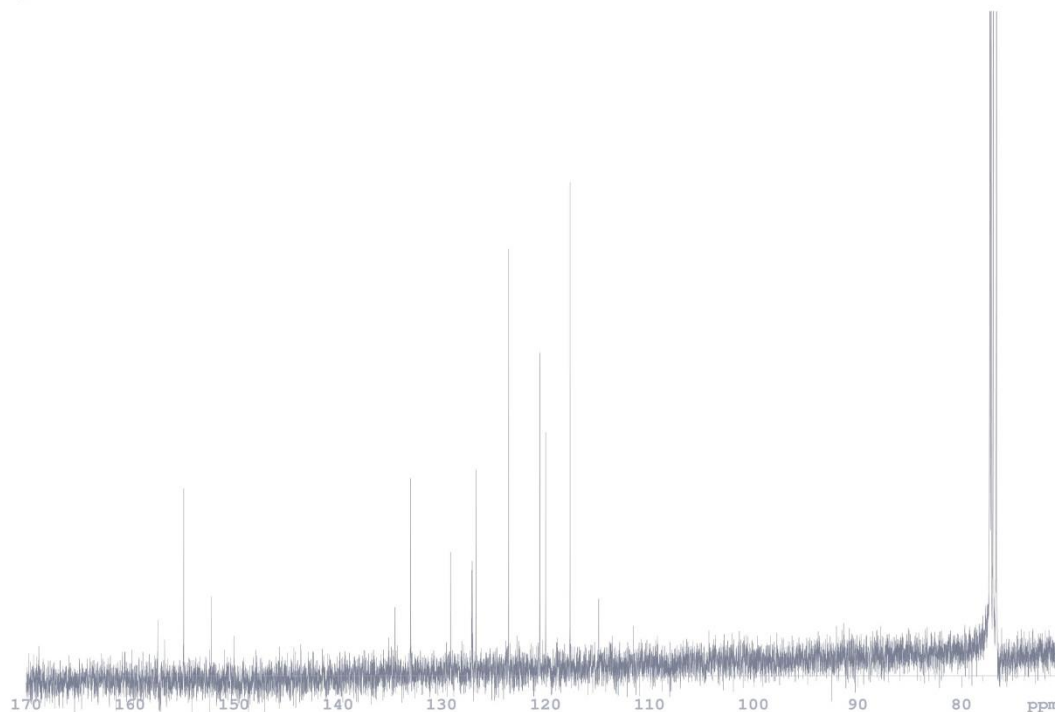
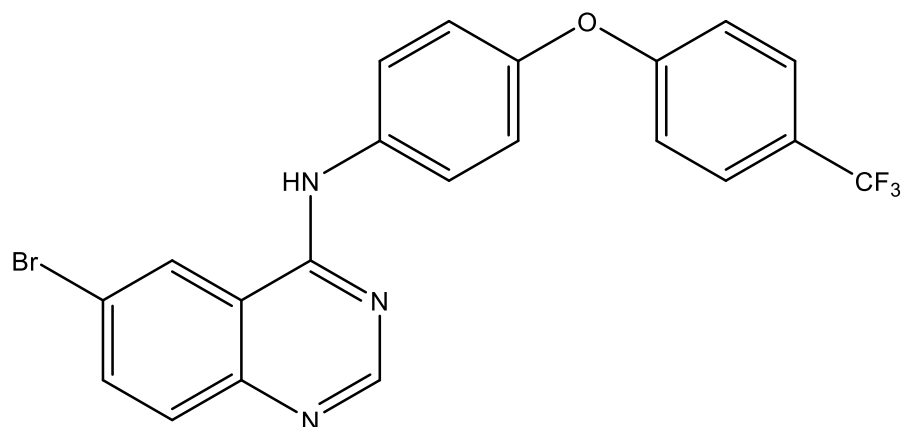


Figure 5.3. ^{13}C -NMR spectrum of H-EVP1.

N-(4-(4-(trifluoromethyl)phenoxy)phenyl)quinazolin-4-amine (Br-EVP1), 3.10



^1H -NMR (400 MHz, CDCl_3) δ ppm 8.766 (s, 1H), 8.094-8.089 (d, 1H), 7.897-7.869 (dd, 1H), 7.821-7.799 (d, 1H), 7.758-7.735 (d, 2H), 7.599-7.577 (d, 2H), 7.528 (br. s, 1H), 7.137-7.074 (m, 4H).

^{13}C -NMR (100 MHz, CDCl_3) δ ppm 206.966, 156.889, 155.076, 152.268, 148.640, 136.210, 134.693, 130.367, 127.142, 127.104, 127.066, 127.028, 123.909, 120.366, 119.743, 117.725.

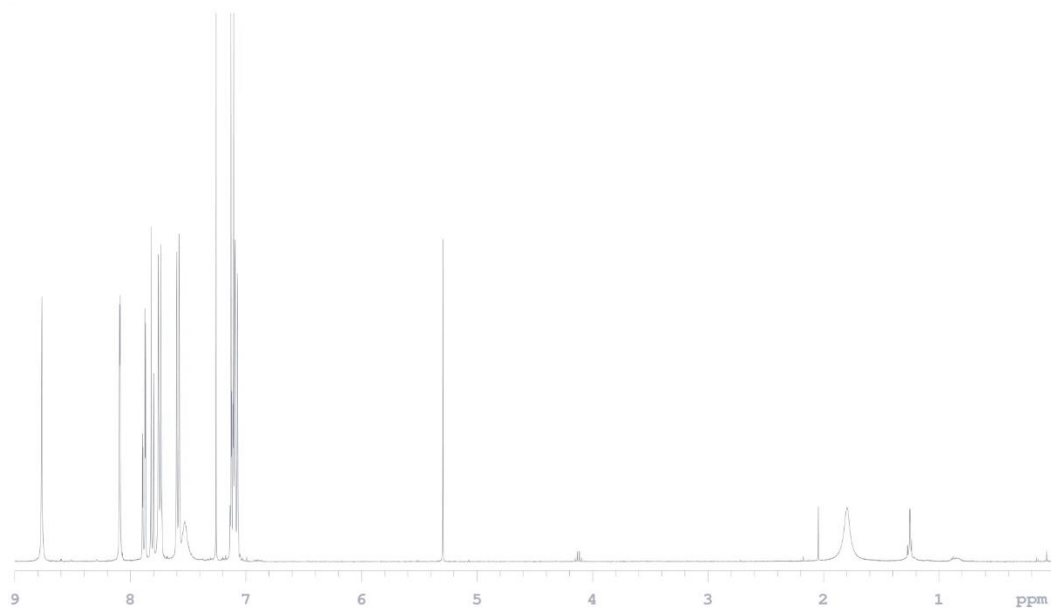


Figure 5.4. ^1H -NMR spectrum of Br-EVP1.

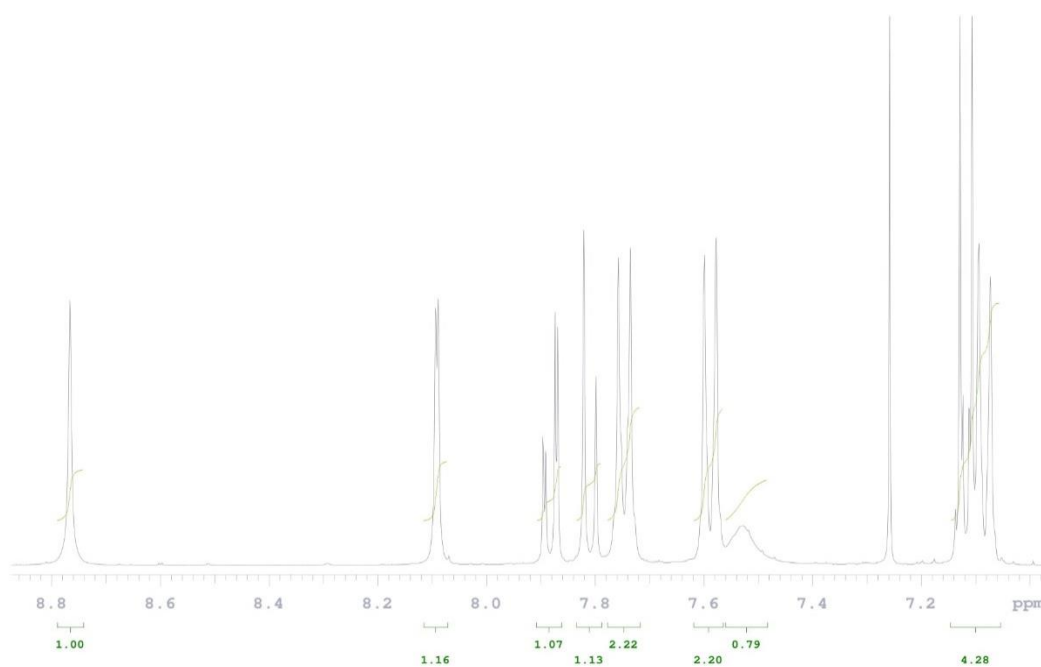


Figure 5.5. Zoom of ^1H -NMR aromatic region of Br-EVP1.

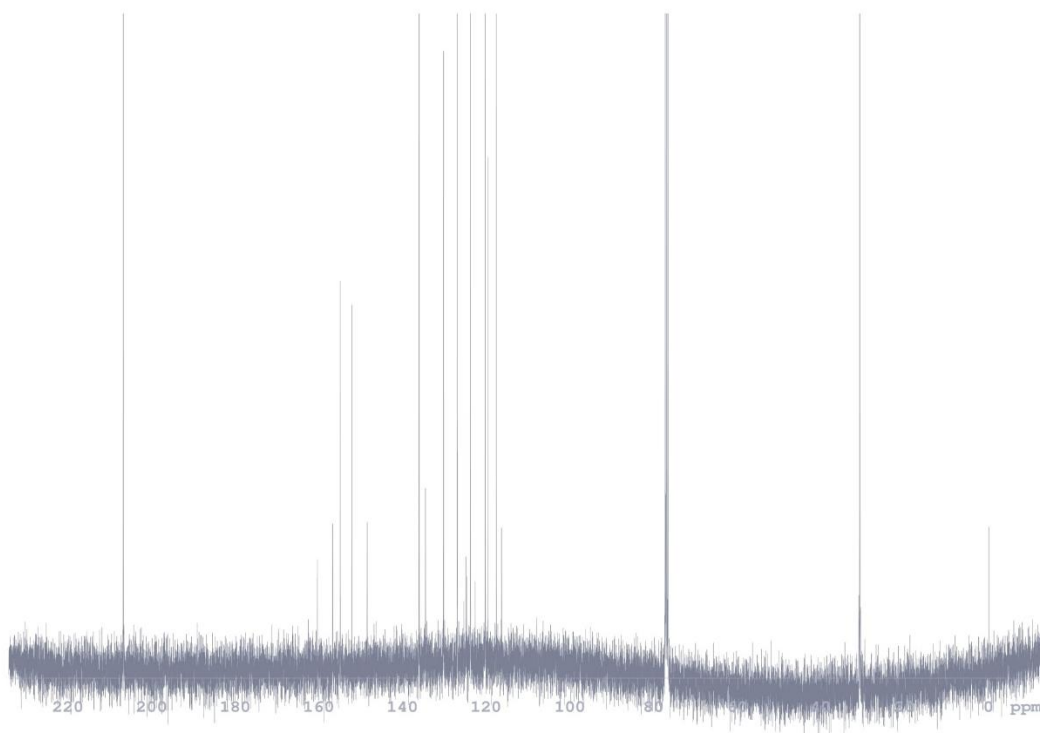
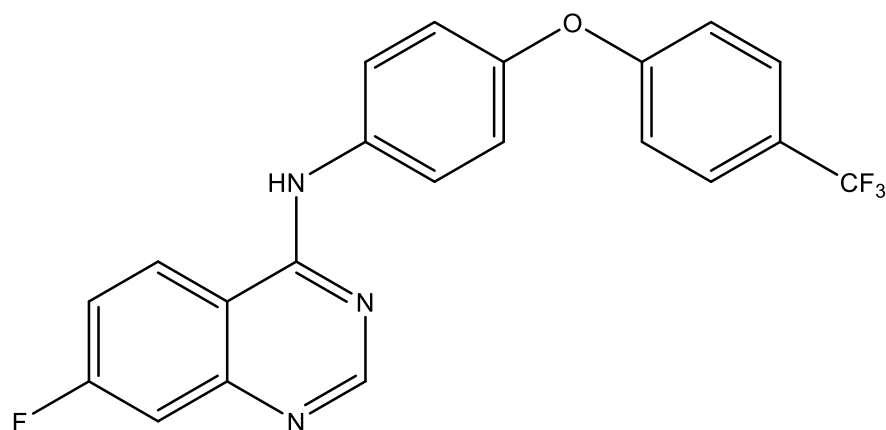


Figure 5.6. ^{13}C -NMR spectrum of Br-EVP1.

7-fluoro-*N*-(4-(4-(trifluoromethyl)phenoxy)phenyl)quinazolin-4-amine (F-EVP(A)1), 3.15



^1H -NMR (400 MHz, CDCl_3) δ ppm 8.756 (s, 1H), 7.941-7.904 (q, 1H), 7.756-7.716 (m, 2H), 7.602-7.547 (m, 3H), 7.431 (br. s, 1H), 7.362-7.313 (m, 1H), 7.144-7.077 (m, 4H).

^{13}C -NMR (100 MHz, CDCl_3) δ ppm 156.009, 152.571, ~152.571, 134.260, 127.180, 127.142, 123.894, ~123.894, 122.839, 122.741, ~122.741, 120.555, 117.823, 116.662, 116.420, 113.430, 113.225.

EI-MS: m/z 399.1 [M^+] found at peak (retention time) from 25.999-27.523 min.

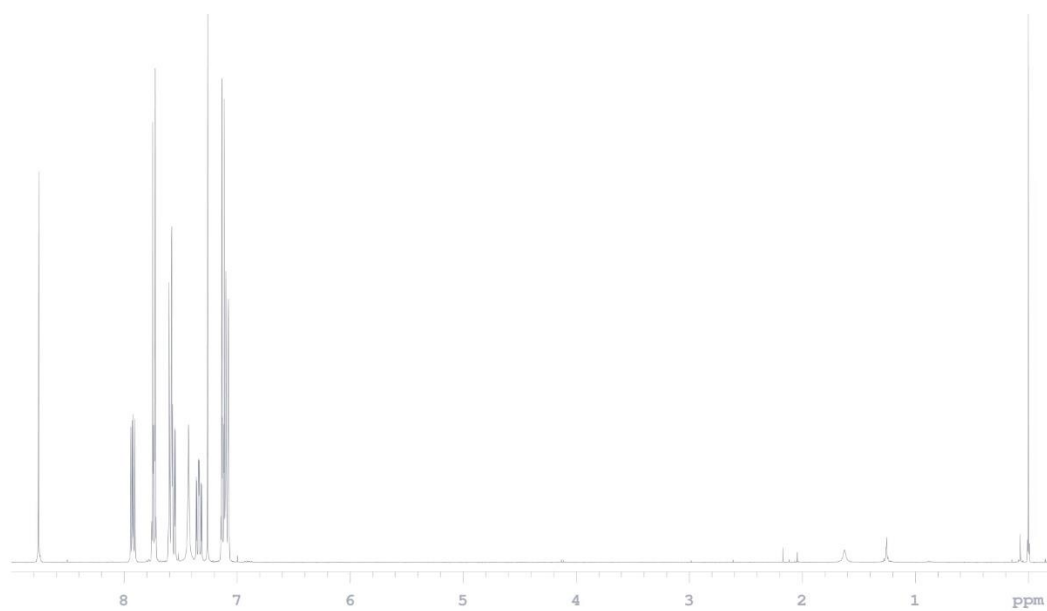


Figure 5.7. ^1H -NMR spectrum of F-EVP(A)1.

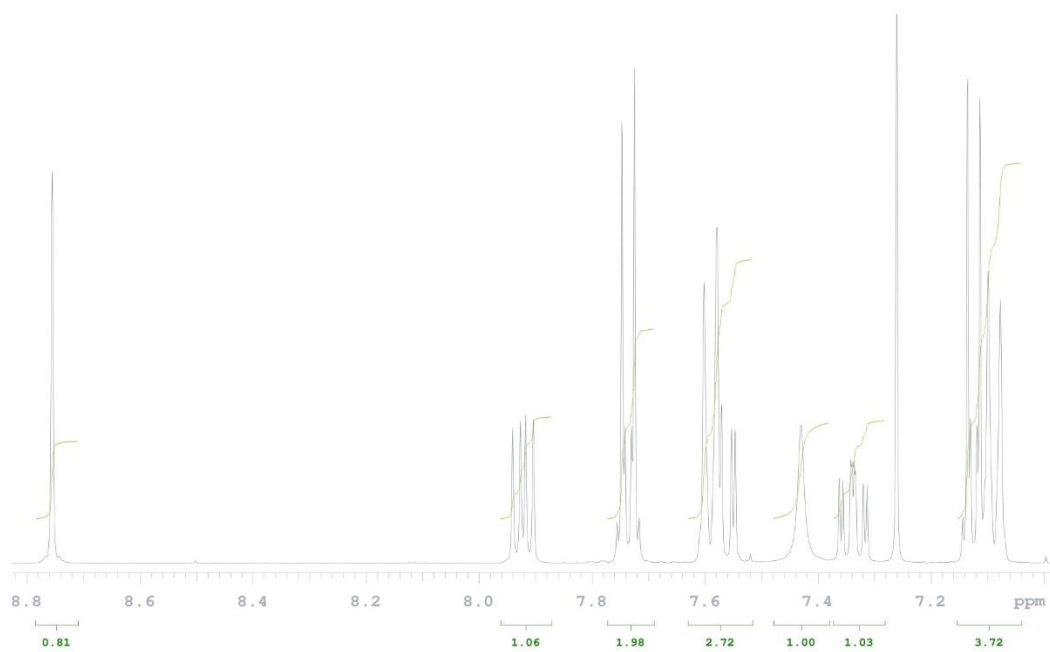


Figure 5.8. Zoom of ^1H -NMR aromatic region of F-EVP(A)1.

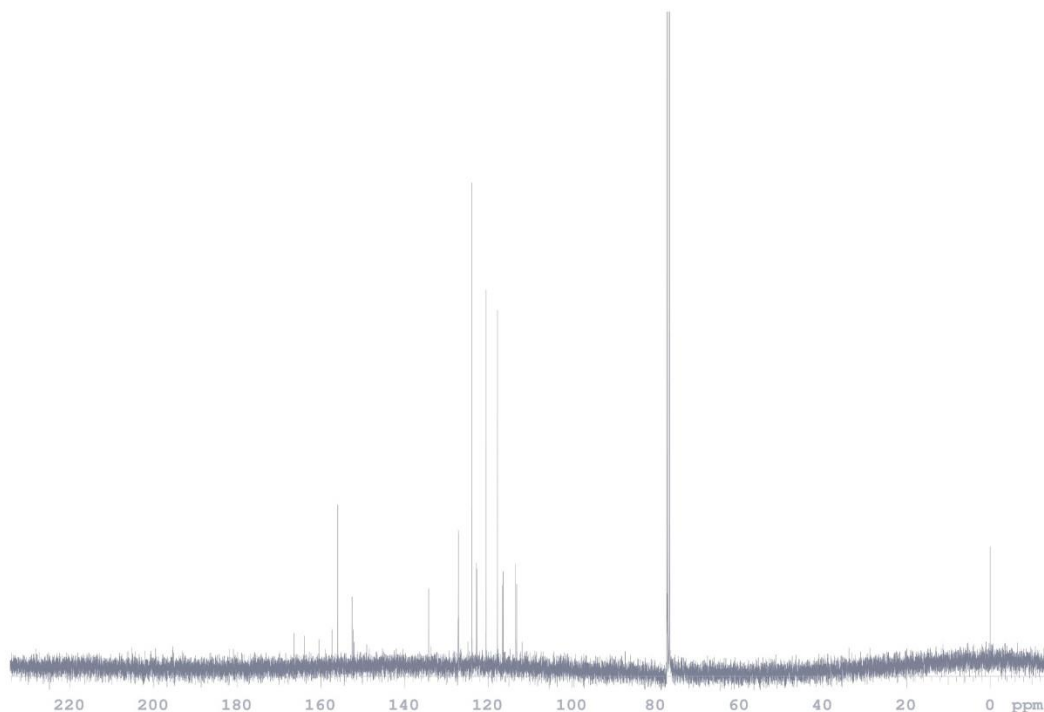
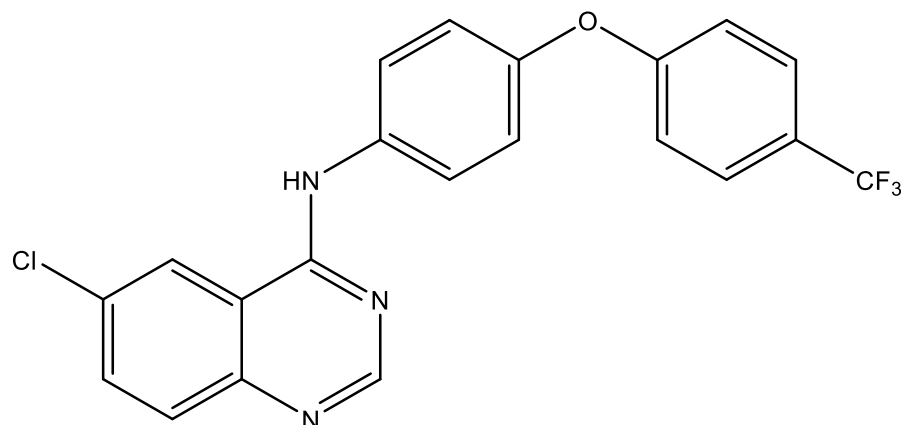


Figure 5.9. ^{13}C -NMR spectrum of F-EVP(A)1.

6-chloro-N-(4-(4-(trifluoromethyl)phenoxy)phenyl)quinazolin-4-amine (Cl-EVP1), 3.11



^1H -NMR (400 MHz, CDCl_3) δ ppm 8.763 (s, 1H), 7.898-7.877 (m, 2H), 7.776-7.733 (m, 3H), 7.604-7.582 (d, 2H), 7.378 (br. s, 1H), 7.150-7.080 (m, 4H).

^{13}C -NMR (100 MHz, CDCl_3) δ ppm 156.669, 155.068, 152.579, 148.587, 134.162, 133.820, 132.287, 130.800, 127.233, 127.195, 127.157, 127.119, 123.849, 120.570, 119.728, 117.831, 115.661.

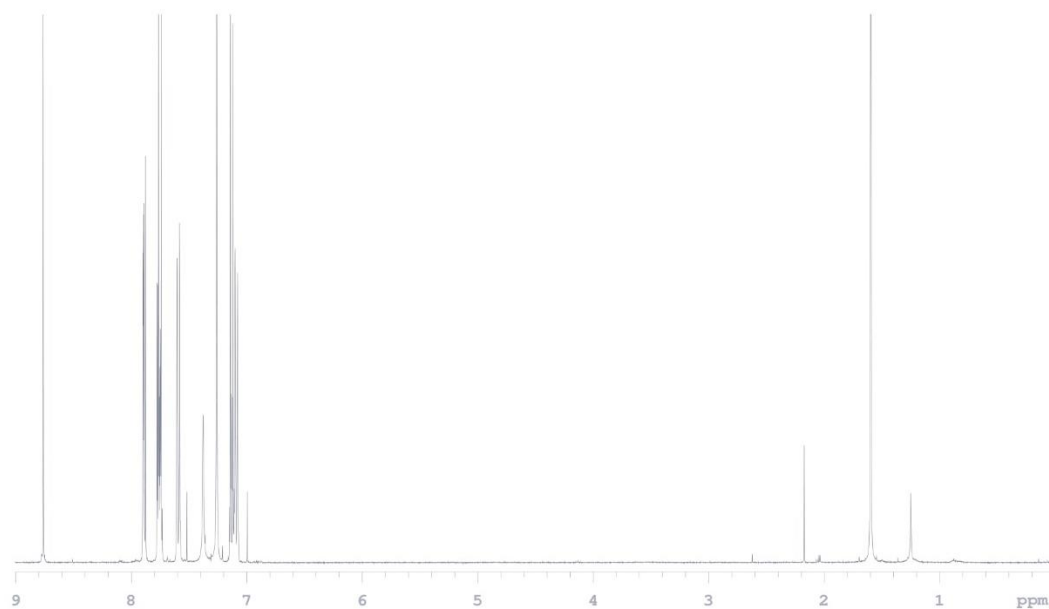


Figure 5.10. ^1H -NMR spectrum of Cl-EVP1.

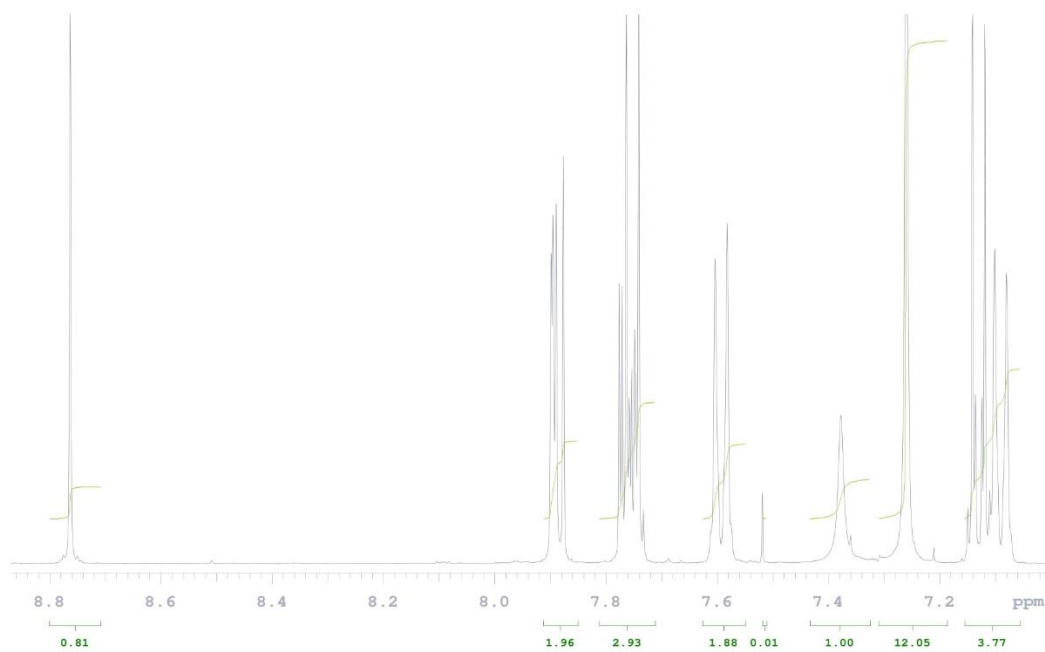


Figure 5.11. Zoom of ^1H -NMR aromatic region of Cl-EVP1.

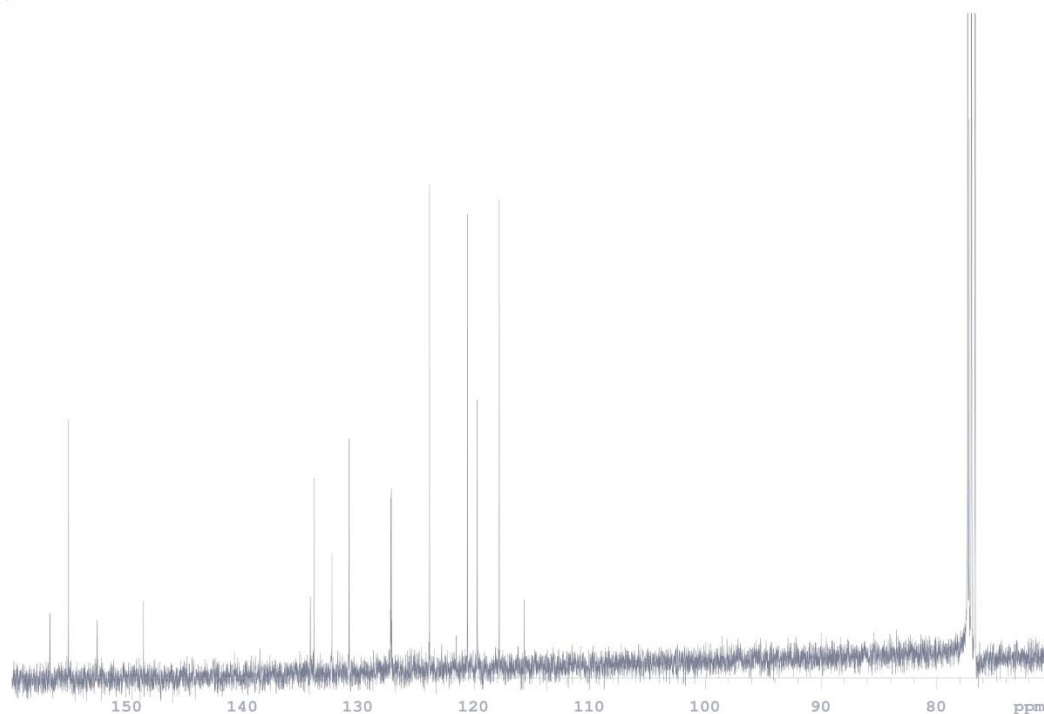
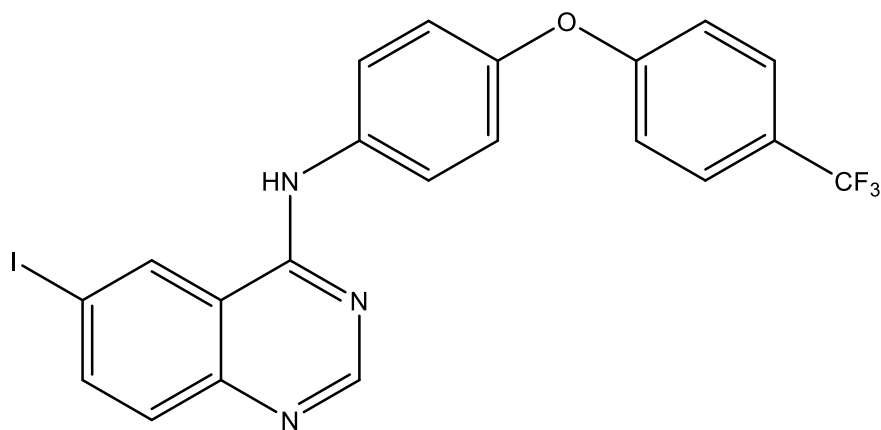


Figure 5.12. ^{13}C -NMR spectrum of Cl-EVP1.

6-iodo-*N*-(4-(4-(trifluoromethyl)phenoxy)phenyl)quinazolin-4-amine (I-EVP1), 3.12



^1H -NMR (400 MHz, CDCl_3) δ ppm 8.777 (s, 1H), 8.268-8.264 (d, 1H), 8.066-8.039 (dd, 1H), 7.768-7.729 (m, 2H), 7.674-7.652 (d, 1H), 7.603-7.581 (d, 2H), 7.454 (br. s, 1H), 7.141-7.076 (m, 4H).

^{13}C -NMR (100 MHz, CDCl_3) δ ppm 156.191, 155.258, 152.624, 149.225, 141.758, 134.162, 130.792, 129.457, 127.226, 127.188, 127.150, 127.112, 123.879, 120.517, 117.854, 116.807, 91.021.

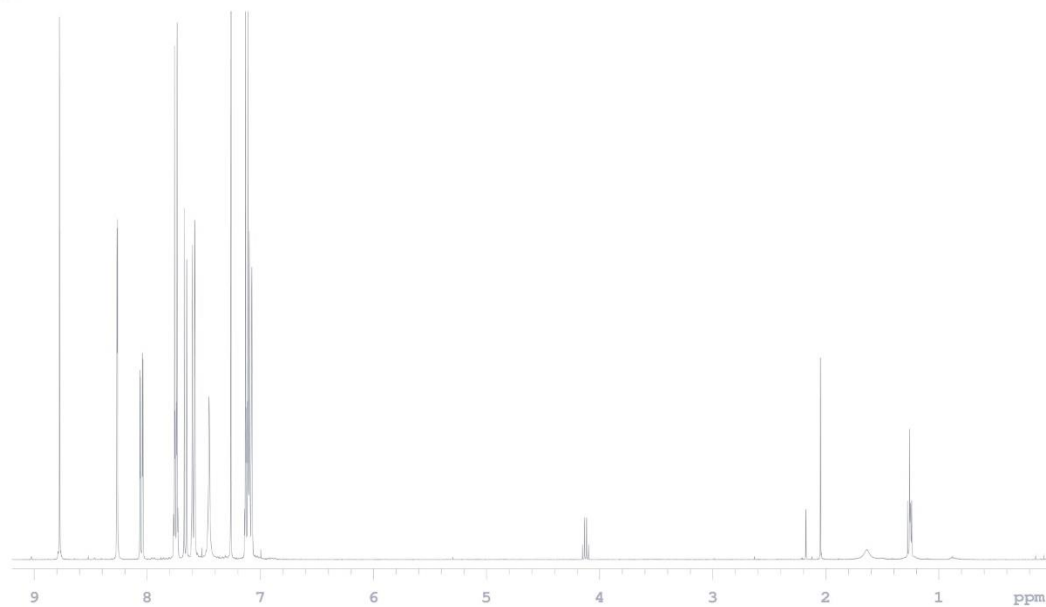


Figure 5.13. ^1H -NMR spectrum of I-EVP1.

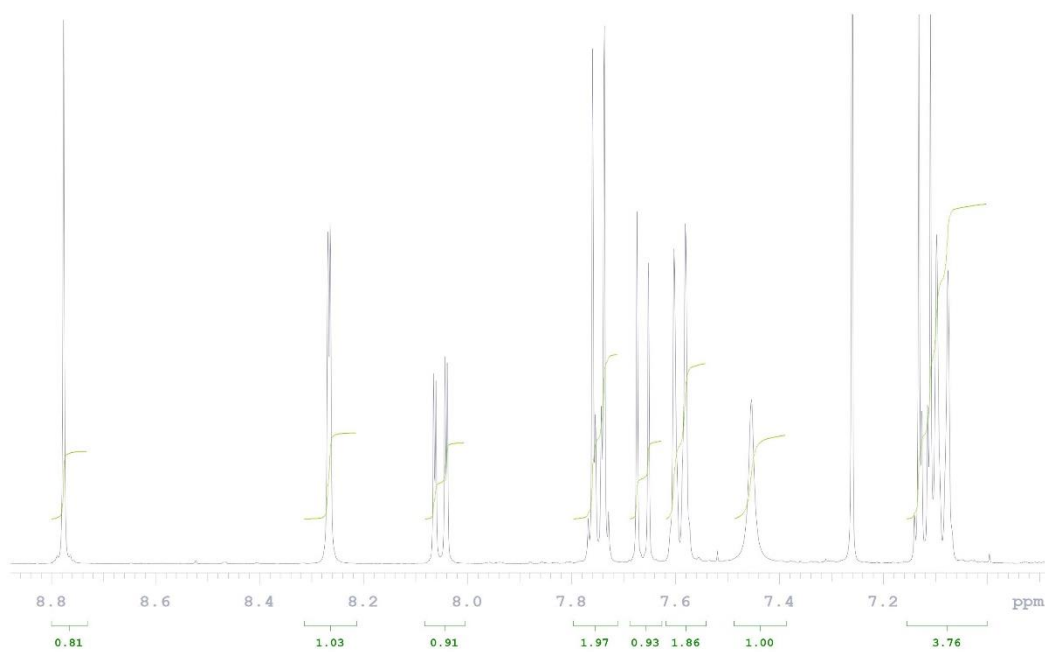


Figure 5.14. Zoom of ^1H -NMR aromatic region of I-EVP1.

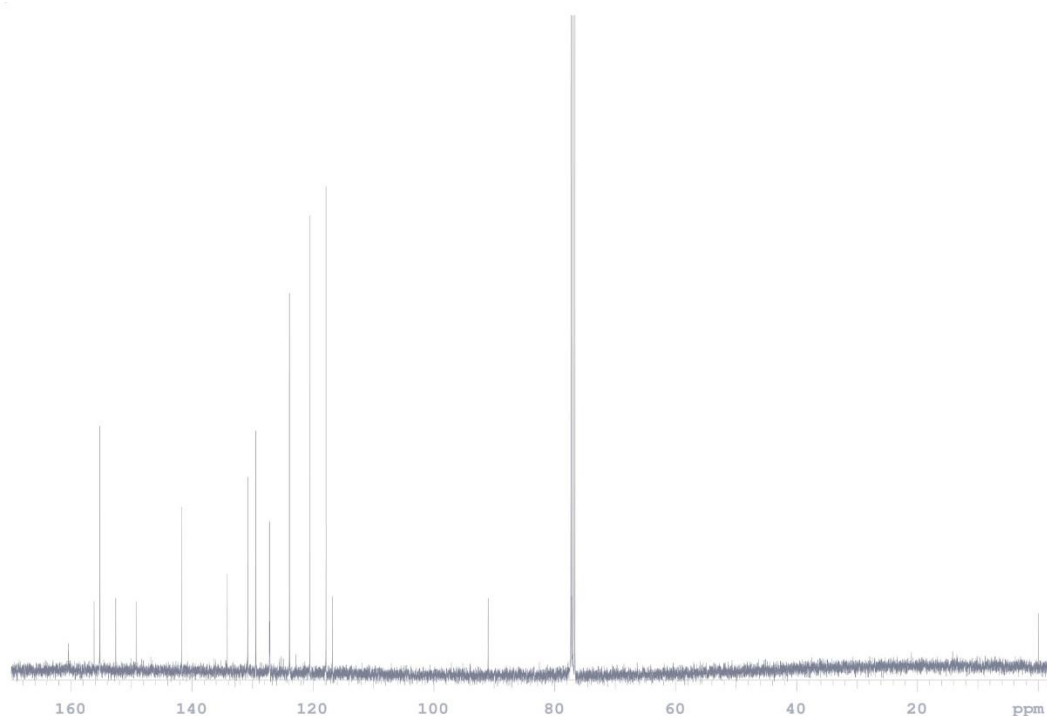


Figure 5.15. ^{13}C -NMR spectrum of I-EVP1.

5.9 BIOLOGICAL METHODS

Primary Genetic Knockout (KO) Screen to Test for EVP4593-Sensitive Strains

A knockout (KO) strain is a strain of *S. cerevisiae* with one mutated/nonfunctional gene such that the strain lacks some regular piece of cellular machinery. KO strains were pinned in a 96W plate with 180 μL YEP G/E per well and allowed to grow up at 30°C. The use of YEP G/E is important as this media lacks dextrose, preventing glycolysis and requiring the yeast to rely solely upon the ETC to generate ATP. Then, strains were spotted from the 96W plate to either a control (YEP G/E) or an experimental (YEP G/E + 15 μM EVP4593) plate and allowed to grow up at 30°C. The growth of each strain was then compared between the control and experimental plates. The concentration of EVP4593 used was determined by determining a sublethal concentration when treating *pdr5* Δ , a strain that lacks a multidrug transporter gene, thus preventing toxin transport

out of the cell. There were ~115 strains whose growth was inhibited by EVP4593, demarcating them as sensitive strains.

Serial Dilution Spotting Assay

The sensitive *S. cerevisiae* mutants were serially diluted in a 96W plate (1:10, 1:100, 1:1000, and 1:10000). Mutants were then spotted onto either a control (G/E) or an experimental (G/E + EVP4593) plate. Strains were allowed to grow at 30°C and then assessed for sensitivity by growth.

REFERENCES

- (1) Ma, W.-D.; Zou, Y.-P.; Wang, P.; Yao, X.-H.; Sun, Y.; Duan, M.-H.; Fu, Y.-J.; Yu, B. Chimaphilin Induces Apoptosis in Human Breast Cancer MCF-7 Cells through a ROS-Mediated Mitochondrial Pathway. *Food Chem. Toxicol.* **2014**, *70*, 1–8. <https://doi.org/10.1016/j.fct.2014.04.014>.
- (2) Dong, F.; Liu, T.; Jin, H.; Wang, W. Chimaphilin Inhibits Human Osteosarcoma Cell Invasion and Metastasis through Suppressing the TGF-B1-Induced Epithelial-to-Mesenchymal Transition Markers via PI-3K/Akt, ERK1/2, and Smad Signaling Pathways. *Can. J. Physiol. Pharmacol.* **2018**, *96* (1), 1–7. <https://doi.org/10.1139/cjpp-2016-0522>.
- (3) Krishnathas, R.; Bonke, E.; Dröse, S.; Zickermann, V.; Nasiri, H. R. Identification of 4-N-[2-(4-Phenoxyphenyl)Ethyl]Quinazoline-4,6-Diamine as a Novel, Highly Potent and Specific Inhibitor of Mitochondrial Complex I. *MedChemComm* **2017**, *8* (3), 657–661. <https://doi.org/10.1039/C6MD00655H>.
- (4) Wess, G.; Urmann, M.; Sickenberger, B. Medicinal Chemistry: Challenges and Opportunities. *Angew. Chem. Int. Ed.* **2001**, *40* (18), 3341–3350. [https://doi.org/10.1002/1521-3773\(20010917\)40:18<3341::AID-ANIE3341>3.0.CO;2-D](https://doi.org/10.1002/1521-3773(20010917)40:18<3341::AID-ANIE3341>3.0.CO;2-D).
- (5) Angerer, H.; Nasiri, H. R.; Niedergesäß, V.; Kersch, S.; Schwalbe, H.; Brandt, U. Tracing the Tail of Ubiquinone in Mitochondrial Complex I. *Biochim. Biophys. Acta BBA - Bioenerg.* **2012**, *1817* (10), 1776–1784. <https://doi.org/10.1016/j.bbabi.2012.03.021>.
- (6) Neupane, P.; Bhujju, S.; Thapa, N.; Bhattarai, H. K. ATP Synthase: Structure, Function and Inhibition. *BioMol Concepts* **2019**, *10*, 1–10.
- (7) Mirams, G. *Should I work with IC50s or pIC50s?*. Mathematical Matters of the Heart. <https://mirams.wordpress.com/2016/06/13/should-i-work-with-ic50s-or-pic50s/> (accessed 2022-12-05).
- (8) Han, Z.; Angerer, H.; Bischoff, I.; Qin, Y.; Stegmann, D.; Tuz, K.; Fritz, G.; Juarez, O.; Fürst, R.; Lashley, D.; Nasiri, H. R. Concise Synthesis of 1,4-Benzoquinone-Based Natural Products as Mitochondrial Complex I Substrates and Substrate-Based Inhibitors. *ChemMedChem* **2020**, *15*, 2491–2499.
- (9) Cragg, G. M. Paclitaxel (Taxol®): A Success Story with Valuable Lessons for Natural Product Drug Discovery and Development. *Med. Res. Rev.* **1998**, *18* (5), 315–331. [https://doi.org/10.1002/\(SICI\)1098-1128\(199809\)18:5<315::AID-MED3>3.0.CO;2-W](https://doi.org/10.1002/(SICI)1098-1128(199809)18:5<315::AID-MED3>3.0.CO;2-W).
- (10) Newman, D. J.; Cragg, G. M. Natural Products as Sources of New Drugs over the Nearly Four Decades from 01/1981 to 09/2019. *J. Nat. Prod.* **2020**, *83* (3), 770–803. <https://doi.org/10.1021/acs.jnatprod.9b01285>.
- (11) Dias, D. A.; Urban, S.; Roessner, U. A Historical Overview of Natural Products in Drug Discovery. *Metabolites* **2012**, *2* (2), 303–336. <https://doi.org/10.3390/metabo2020303>.
- (12) Papini, A. M. From Morphine to Endogenous Opioid Peptides, e.g., Endorphins: The Endless Quest for the Perfect Painkiller. 11.
- (13) Thornburg, C. C.; Britt, J. R.; Evans, J. R.; Akee, R. K.; Whitt, J. A.; Trinh, S. K.; Harris, M. J.; Thompson, J. R.; Ewing, T. L.; Shipley, S. M.; Grothaus, P. G.; Newman, D. J.; Schneider, J. P.; Grkovic, T.; O’Keefe, B. R. NCI Program for Natural Product Discovery: A Publicly-Accessible Library of Natural Product Fractions for High-Throughput Screening. **2021**, 32.
- (14) Division of Cancer Treatment & Diagnosis. *The NCI Program for Natural Product Discovery (NPNPD) Prefractionated Library*. National Cancer Institute.

- https://ntp.cancer.gov/organization/ntp/ntpnpd_prefractionated_library.htm#:~:text=Launched%20in%20January%202019%2C%20326%2C000%20natural%20product%20fractions,product-based%20research%20Prefractionate%20more%20than%20125%2C000%20crude%20extracts (accessed 2022-12-05).
- (15) Darakhshan, S.; Bidmeshki Pour, A.; Hosseinzadeh Colagar, A.; Sisakhtnezhad, S. Thymoquinone and Its Therapeutic Potentials. *Pharmacol. Res.* **2015**, 95–96, 138–158. <https://doi.org/10.1016/j.phrs.2015.03.011>.
 - (16) Awtry, E. H.; Loscalzo, J. Aspirin. *Circulation* **2000**, 101, 1206–1218.
 - (17) The International Natural Product Sciences Taskforce; Atanasov, A. G.; Zotchev, S. B.; Dirsch, V. M.; Supuran, C. T. Natural Products in Drug Discovery: Advances and Opportunities. *Nat. Rev. Drug Discov.* **2021**, 20 (3), 200–216. <https://doi.org/10.1038/s41573-020-00114-z>.
 - (18) Iiyama, S.; Fukaya, K.; Yamaguchi, Y.; Watanabe, A.; Yamamoto, H.; Mochizuki, S.; Saio, R.; Noguchi, T.; Oishi, T.; Sato, T.; Chida, N. Total Synthesis of Paclitaxel. *Org. Lett.* **2022**, 24 (1), 202–206. <https://doi.org/10.1021/acs.orglett.1c03851>.
 - (19) Mayor, S. Tree That Provides Paclitaxel Is Put on List of Endangered Species. *BMJ* **2011**, 343 (nov15 3), d7411–d7411. <https://doi.org/10.1136/bmj.d7411>.
 - (20) El-Najjar, N.; Gali-Muhtasib, H.; Ketola, R. A.; Vuorela, P.; Urtti, A.; Vuorela, H. The Chemical and Biological Activities of Quinones: Overview and Implications in Analytical Detection. *Phytochem. Rev.* **2011**, 10 (3), 353–370. <https://doi.org/10.1007/s11101-011-9209-1>.
 - (21) Dhakal, D.; Lim, S.-K.; Kim, D. H.; Kim, B.-G.; Yamaguchi, T.; Sohng, J. K. Complete Genome Sequence of *Streptomyces Peucetius* ATCC 27952, the Producer of Anticancer Anthracyclines and Diverse Secondary Metabolites. *J. Biotechnol.* **2018**, 267, 50–54. <https://doi.org/10.1016/j.jbiotec.2017.12.024>.
 - (22) Mladěnka, P.; Macáková, K.; Kujovská Krčmová, L.; Javorská, L.; Mrštná, K.; Carazo, A.; Protti, M.; Remião, F.; Nováková, L.; the OEMONOM researchers and collaborators. Vitamin K – Sources, Physiological Role, Kinetics, Deficiency, Detection, Therapeutic Use, and Toxicity. *Nutr. Rev.* **2022**, 80 (4), 677–698. <https://doi.org/10.1093/nutrit/nuab061>.
 - (23) Botanical Society of Britain and Ireland. *Pyrola media*. Online Atlas of the British and Irish Flora. <https://plantatlas.brc.ac.uk/plant/pyrola-media> (accessed 2022-12-07).
 - (24) University of Texas. *PASSIFLORACEAE*. http://www.bio.utexas.edu/courses/bio406d/images/pics/pas/passiflora_incarnata.htm (accessed 2022-12-07).
 - (25) Houk, K. N. Generalized Frontier Orbitals of Alkenes and Dienes. Regioselectivity in Diels-Alder Reactions. *J. Am. Chem. Soc.* **1973**, 95 (12), 4092–4094. <https://doi.org/10.1021/ja00793a069>.
 - (26) *Regiochemistry of the Diels-Alder Reaction with Practice Problems*. Chemistry Steps. <https://www.chemistrysteps.com/diels-alder-regioselectivity/> (accessed 2022-12-05).
 - (27) Molčanov, K.; Kojić-Prodić, B. Towards Understanding π -Stacking Interactions between Non-Aromatic Rings. *IUCrJ* **2019**, 6 (2), 156–166. <https://doi.org/10.1107/S2052252519000186>.
 - (28) The Cambridge Crystallographic Data Centre. ConQuest.

- (29) Tocilescu, M. A.; Fendel, U.; Zwicker, K.; Kerscher, S.; Brandt, U. Exploring the Ubiquinone Binding Cavity of Respiratory Complex I. *J. Biol. Chem.* **2007**, *282* (40), 29514–29520. <https://doi.org/10.1074/jbc.M704519200>.
- (30) Wu, J.; Ryskamp, D. A.; Liang, X.; Egorova, P.; Zakharova, O.; Hung, G.; Bezprozvanny, I. Enhanced Store-Operated Calcium Entry Leads to Striatal Synaptic Loss in a Huntington's Disease Mouse Model. *J. Neurosci.* **2016**, *36* (1), 125–141. <https://doi.org/10.1523/JNEUROSCI.1038-15.2016>.
- (31) Liu, M.; Landuyt, B.; Klaassen, H.; Geldhof, P.; Luyten, W. Screening of a Drug Repurposing Library with a Nematode Motility Assay Identifies Promising Anthelmintic Hits against *Cooperia Oncophora* and Other Ruminant Parasites. *Vet. Parasitol.* **2019**, *265*, 15–18. <https://doi.org/10.1016/j.vetpar.2018.11.014>.
- (32) Tobe, M.; Isobe, Y.; Tomizawa, H.; Nagasaki, T.; Takahashi, H.; Fukazawa, T.; Hayashi, H. Discovery of Quinazolines as a Novel Structural Class of Potent Inhibitors of NF- κ B Activation. *Bioorg Med Chem* **2003**, *9*.
- (33) Karan, R.; Agarwal, P.; Sinha, M.; Mahato, N. Recent Advances on Quinazoline Derivatives: A Potential Bioactive Scaffold in Medicinal Chemistry. *ChemEngineering* **2021**, *5* (4), 73. <https://doi.org/10.3390/chemengineering5040073>.
- (34) Okun, J. G.; Lümmer, P.; Brandt, U. Three Classes of Inhibitors Share a Common Binding Domain in Mitochondrial Complex I (NADH:Ubiquinone Oxidoreductase). *J. Biol. Chem.* **1999**, *274* (5), 2625–2630. <https://doi.org/10.1074/jbc.274.5.2625>.
- (35) Murai, M.; Mashimo, Y.; Hirst, J.; Miyoshi, H. Exploring Interactions between the 49 KDa and ND1 Subunits in Mitochondrial NADH-Ubiquinone Oxidoreductase (Complex I) by Photoaffinity Labeling. *Biochemistry* **2011**, *50* (32), 6901–6908. <https://doi.org/10.1021/bi200883c>.
- (36) Asif, M. Chemical Characteristics, Synthetic Methods, and Biological Potential of Quinazoline and Quinazolinone Derivatives. *Int. J. Med. Chem.* **2014**, *2014*, 1–27. <https://doi.org/10.1155/2014/395637>.
- (37) Nair, A. S.; Singh, A. K.; Kumar, A.; Kumar, S.; Sukumaran, S.; Koyiparambath, V. P.; Pappachen, L. K.; Rangarajan, T. M.; Kim, H.; Mathew, B. FDA-Approved Trifluoromethyl Group-Containing Drugs: A Review of 20 Years. *Processes* **2022**, *10* (10), 2054. <https://doi.org/10.3390/pr10102054>.
- (38) Lowe, D. *Trifluoromethylate The Lot of 'Em*. Science. <https://www.science.org/content/blog-post/trifluoromethylate-lot-em> (accessed 2022-12-05).
- (39) Lee, B. S.; Hards, K.; Engelhart, C. A.; Hasenoehrl, E. J.; Kalia, N. P.; Mackenzie, J. S.; Sviriaeva, E.; Chong, S. M. S.; Manimekalai, M. S. S.; Koh, V. H.; Chan, J.; Xu, J.; Alonso, S.; Miller, M. J.; Steyn, A. J. C.; Grüber, G.; Schnappinger, D.; Berney, M.; Cook, G. M.; Moraski, G. C.; Pethe, K. Dual Inhibition of the Terminal Oxidases Eradicates Antibiotic-tolerant *Mycobacterium Tuberculosis*. *EMBO Mol. Med.* **2021**, *13* (1). <https://doi.org/10.15252/emmm.202013207>.
- (40) Caron, S.; McInturff, E. Nucleophilic Aromatic Substitution. In *Practical Synthetic Organic Chemistry*; Caron, S., Ed.; Wiley, 2020; pp 231–246. <https://doi.org/10.1002/9781119448914.ch4>.
- (41) Mi, H.; Muruganujan, A.; Casagrande, J. T.; Thomas, P. D. Large-Scale Gene Function Analysis with the PANTHER Classification System. *Nat. Protoc.* **2013**, *8* (8), 1551–1566. <https://doi.org/10.1038/nprot.2013.092>.

- (42) Zhang, W.; Chen, X.; Sun, W.; Nie, T.; Quanquin, N.; Sun, Y. Escherichia Coli Increases Its ATP Concentration in Weakly Acidic Environments Principally through the Glycolytic Pathway. *Genes* **2020**, *11* (9), 991. <https://doi.org/10.3390/genes11090991>.
- (43) Sheldrick, G. Crystal Structure Refinement with SHELXL. *Acta Crystallogr. Sect. C* **2015**, *71*, 3–8. <https://doi.org/10.1107/S2053229614024218>.
- (44) Hubschle, C.; Sheldrick, G.; Dittick, B. ShelXle: A Qt Graphical User Interface for SHELXL. *J. Appl. Crystallogr.* **2011**, *44*, 1281–1284. <https://doi.org/10.1107/S0021889811043202>.